Acceleration and demographic rates of bird abundance decline in North America

François Leroy [1,], Marta A. Jarzyna [2,3], Petr Keil [1]*

[1]Department of Spatial Sciences, Faculty of Environmental Sciences, Czech University of Life Sciences Prague, Kamýcká 129, 16500 Praha-Suchdol, Czech Republic

[2] Department of Evolution, Ecology and Organismal Biology, The Ohio State University, Columbus, Ohio, 43210, USA

[3] Translational Data Analytics Institute, The Ohio State University, Columbus, Ohio, 43210, USA

Abstract

Acceleration of human activities over the past century might have caused a corresponding acceleration in the decline of species' abundances, but this has not been empirically assessed. Further, the temporal dynamics of abundance arises from a complex interaction between recruitment and loss of individuals, which remains unexplored across large spatial scales. We address these gaps by examining temporal changes, acceleration, deceleration, and vital processes (*i.e.* recruitment and loss) of abundance across much of the North American avifauna from 1987 to 2021. We confirm the continent-wide decline of bird abundance, and pinpoint the regional hotspots of acceleration of this decline in the Mid-Atlantic region, Midwest, and California, matching broad spatial patterns of human activities. We further reveal that the increasing loss rate of individuals is the primary process responsible for the acceleration of abundance decline in California and the Midwest, whereas a decrease in recruitment rate is also observed in the Mid-Atlantic. Finally, our models show that 67% of bird species and 95% of families with increasing abundances are concurrently experiencing a decline in recruitment rate. This underscores the need for conservation policies even for species that appear to be thriving. Moreover, simply preventing loss may not suffice, as we also need policies that enhance recruitment.

Main text

Over the Anthropocene, human activities have profoundly impacted ecosystems [1], and a closely monitored indicator of this impact is temporal change in local population abundances [2]. Global reports show an overall decline of abundances, with an average per-species abundance decline estimated to be between 20% [1] and 69% (Living Planet Index, LPI; < www.livingplanetindex.org/>, but see [3,4] for criticisms of the LPI). Analyses of local time series show a more complex picture, with some reporting both abundance declines and increases [5–11]. A particularly large number of local times series of abundances are available for birds across North America and Europe, revealing an overall decline [12,13].

The declines of population abundances have been mainly attributed to human activities [14] such as agricultural intensification [12], changes in land-use, overexploitation, and pollution (Convention on Biological Diversity, 2010; < https://www.cbd.int/convention >). The past century, however, has seen not only the increase but also an *acceleration* of the increase of human activities [15,16], often termed the Great Acceleration [17,18], and an acceleration of species loss [19–21]. We should thus expect a corresponding acceleration in population declines, but a comprehensive analysis of rates of local population changes across large spatial extents and multiple species is lacking. In essence, while the first order derivative of population abundance change for the majority of species appears to be a decline, the second order derivative (*i.e.* acceleration or deceleration of this change) remains unexplored.

While examining the temporal changes in population abundance is valuable, there are ecologically informative demographic processes that govern the dynamics. Abundance change in time, ΔN, arises from the difference between recruitment R (*i.e.* number of new individuals entering the population through birth, maturation, or immigration) and loss L (*i.e.* number of individuals removed from the population by death or emigration, Fig. 1A). To facilitate comparisons among populations of varying sizes, the temporal dynamics can be expressed using vital rates, which are per-capita (a.k.a. per-individual) changes. The growth rate g (*i.e.* the per-capita average change over time) results from the difference between recruitment rate r and loss rate l, representing the per-capita probability of a new individual entering a population or disappearing, respectively (Fig. 1A). The interplay between r, l and how they change with time in real-world population dynamics remains unknown for most species, particularly at large spatiotemporal scales. Bridging this knowledge gap would provide deeper insights into the mechanisms of the ongoing biodiversity crisis and help shape effective conservation strategies.

Here, we provide a comprehensive assessment of temporal changes in local population abundances of 234 bird species across North America from 1987 to 2021, focusing on acceleration, deceleration, recruitment, and loss. Using 1,033 routes of the North American Breeding Bird Survey[24] (BBS) and advances in N-mixture population models [22,23], together with full Bayesian inference, we demonstrate widespread bird population declines across North America, pinpoint regions where population declines accelerate or decelerate, and unveil their underlying demographic components. We identify regional acceleration hotspots in the Midwest and California, primarily driven by the increasing loss of individuals, and in the Mid-Atlantic, where decreasing recruitment also emerges as the main process. Finally, we unveil that 69% of species and 95% of avian families with increasing abundances are simultaneously undergoing a decline in recruitment rate, underscoring a hidden vulnerability of seemingly thriving species.

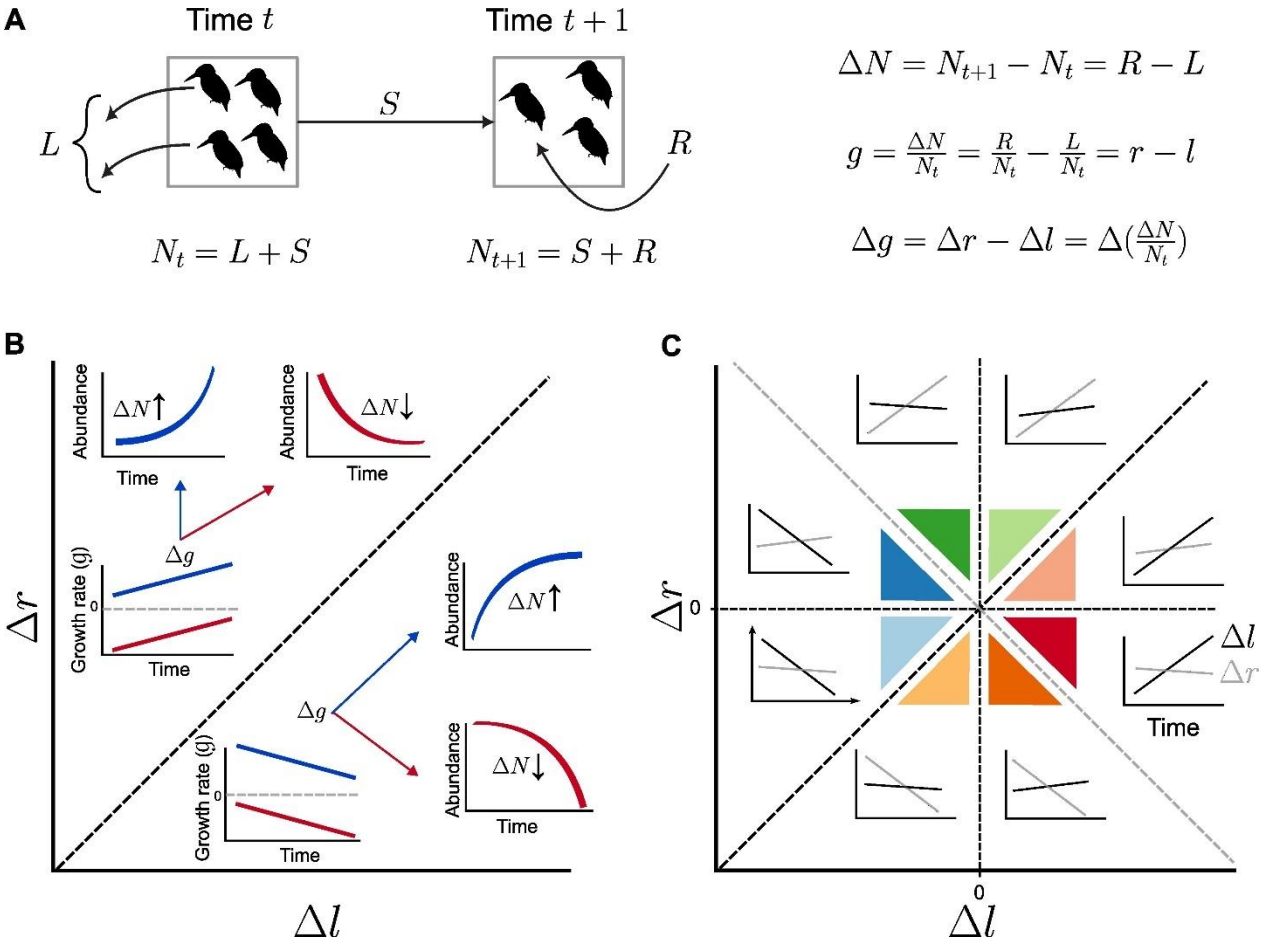

Fig. 1 | Components of temporal change of abundance. (A) Relations between individual abundance (N), number of lost individuals (L), recruited individuals (R), survivors (S), and change in abundance (ΔN). They can be expressed as per-capita rates: growth rate (g), recruitment rate (r), loss rate (l), and their respective change (Δg, Δr, Δl). Importantly, Δg is indicative of acceleration or deceleration of ΔN. (B) Each route, species, family, or habitat type can be mapped onto a $\Delta l \Delta r$ space, indicating a Δg value. Above the black dotted diagonal, growth rate increases (i.e. positive Δg); below, growth rate declines (i.e. negative Δg). Arrows (↑ and ↓) indicate abundance increases (positive ΔN) and declines (negative ΔN); Δg indicate its acceleration or deceleration. (C) In the same $\Delta l \Delta r$ space, colors indicate the dominant process: blue is dominant negative Δl, green is dominant positive Δr, orange is dominant negative Δr and, red is dominant positive Δl. Inset plots show Δl (black line) and Δr (grey line).

Continental decline in bird populations. When looking at the total abundance of individual birds of all species together, the average yearly abundance change per route (ΔN, eq. 13) is a significant decline of $\Delta N = -8.62$ individuals (95% *Credible Interval* $(CI) = [-9.88; -7.38]$, Fig. 2A), representing an average loss of 293 birds (out of 2,159 in 1987, *i.e.* 14%) per route from 1987 to 2021. Of the 1,033 routes surveyed, only 26% (265) experienced a significant increase in total bird abundance, and 72% (741) a significant decrease. Using a spatial smoother to show average regional trends not obscured by local variation, we reveal that bird abundances in Florida, Delaware, New Jersey, and Texas underwent the most pronounced average declines (-14.9, -14.5, -13.7 and -13.5 individuals per route, respectively; Fig. 2B). The change of the per-capita growth rate relative to the size of the initial population in 1987 (Δg_{t1}, eq. 12, 13) was a significant decline (Fig. 2C, $\Delta g_{t1} = -3.3 \times 10^{-3}$, $CI = [-3.7 \times 10^{-3}; -2.8 \times 10^{-3}]$), which is equivalent to a decline of *ca.* 112 birds per 1,000 individuals over 35 years. Arizona, Florida, Texas, and Louisiana experienced the most pronounced negative Δg_{t1} (-6.7×10^{-3}, -6.1×10^{-3},-5.6×10^{-3}, and -5.3×10^{-3} respectively).

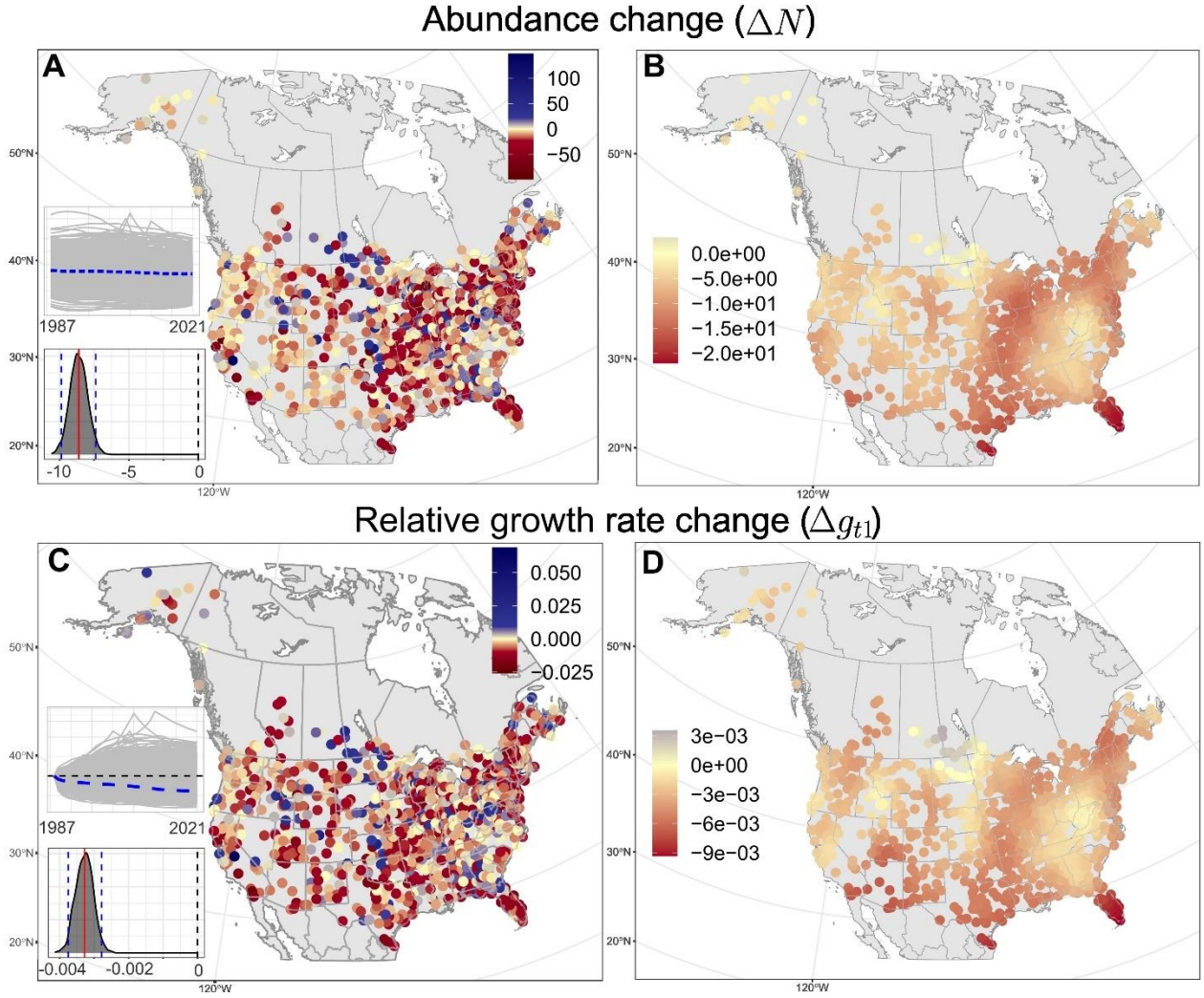

Fig 2 | Temporal change of abundance. (A) Abundance change (ΔN) in bird populations from 1987 to 2021. Each dot represents the random slope of a linear regression between abundance and time for one of the 1,033 routes of the North American Breeding Bird Survey. Inset plots in bottom left show abundance trends for each BBS route in grey, with the average trend in blue dashed line. The inset histograms show the posterior distribution of the grand slope (i.e. overall mean slope across routes), with the red vertical line indicating the mean and the dashed blue lines the 95% credible interval. (C) Temporal change of the relative growth rate (Δg_{t1}) is the per-capita ΔN relative to the size of the initial population in 1987. (B) ΔN, and (D) Δg_{t1}, smoothed using a spatial GAM with a gaussian process smoother. The color palettes of the GAMs have been used on the unsmoothed maps.

Acceleration of the decline. First, there was no significant negative or positive Δg at the scale of the US (Fig. 3A, $\Delta g = -3.16 \times 10^{-6}$, $CI = [-4.94 \times 10^{-5}; 4.35 \times 10^{-5}]$). Concerning the 756 routes with negative ΔN there was *ca.* as many routes with negative and positive Δg (Fig. 3A), indicative of no trend toward either acceleration or deceleration of the decline (Appendix A Fig. 1). The spatial smoothing helps with the interpretation of Δg (Fig. 3B): the fact that the great majority of ΔN is negative (Fig. 2B) suggests that Δg is indicative of either acceleration ($\Delta g < 0$) or deceleration ($\Delta g > 0$) of the decline. Here again, there were *ca.* as many routes with positive and negative Δg (Appendix A Fig. 2), however the spatial smoothing uncovers variation of regionally averaged Δg. The Mid-Atlantic region of the US (Delaware, Maryland, and New Jersey), the Midwest (especially Indiana, Ohio, Kentucky, Illinois, Wisconsin, and Michigan), and California had negative Δg, indicative of an acceleration of the abundance decline. Conversely, Yukon, New England (Connecticut, Massachusetts, Maine, New Hampshire), Atlantic Canada (New Brunswick, Prince Edward Island, and Nova Scotia), New Mexico, and South Carolina showed a positive Δg, indicating a deceleration of population decline.

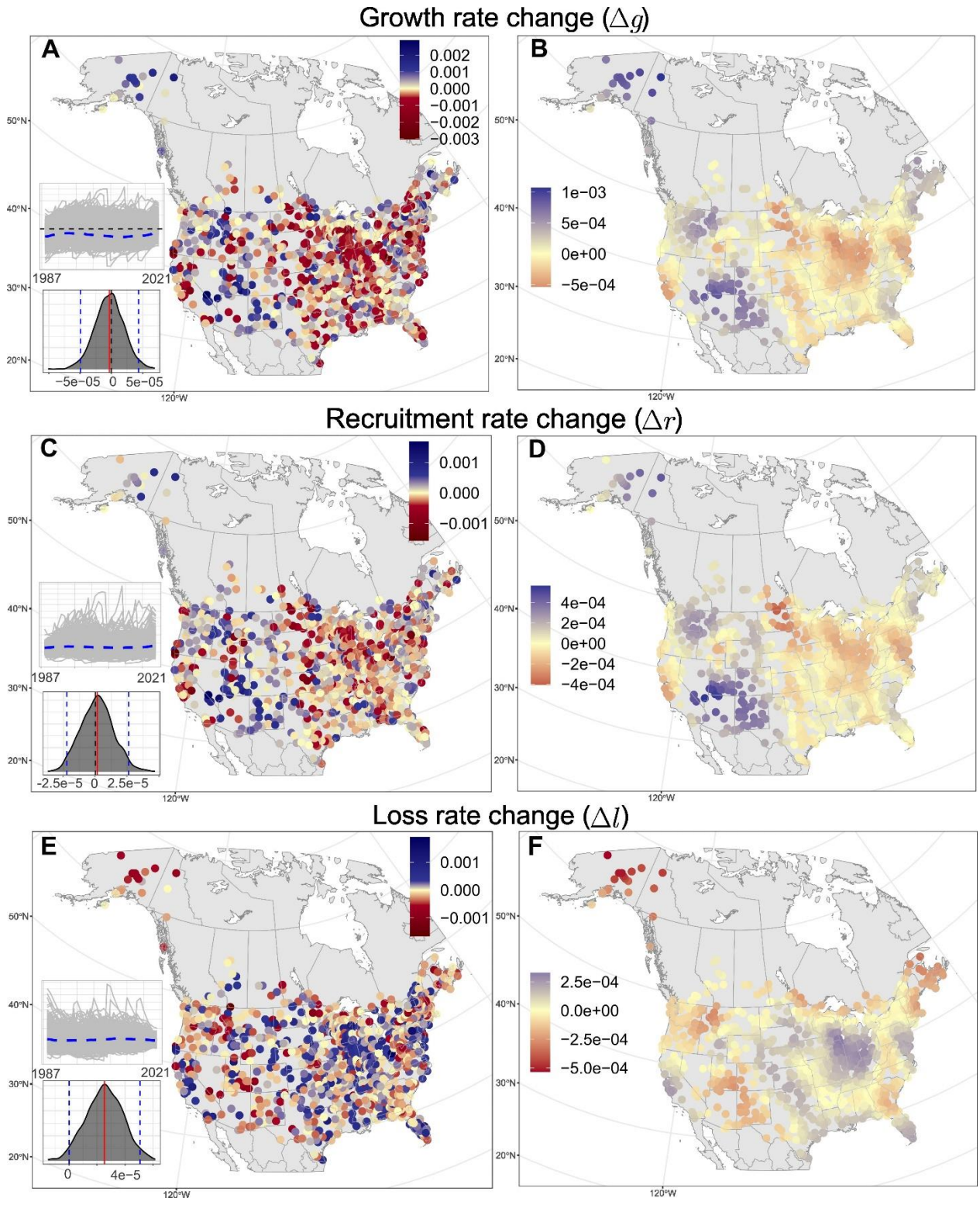

Fig. 3 | Temporal change of per-capita vital rates. (A)(B) Temporal change of yearly growth rate (Δg) decomposed into (C)(D) temporal change of recruitment rate (Δr), and (E)(F) temporal change of loss rate (Δl). Panels on the left (A)(C)(E) show values in each specific Breeding Bird Survey (BBS) route. Panels on the right (B)(D)(F) show regional means obtained from spatial smoothing (using GAM) of the values in the left panels. As abundances are decreasing for most of the routes, the smoothed map (B) shows regional hotspots of acceleration of bird population decline (in red). Inset plots in bottom left show trends in growth, recruitment, and loss rates for each BBS route in grey, with the average trend in blue dashed line. The histograms show the

posterior distributions of the grand slope with the red vertical line indicating the mean and the dashed blue lines the 95% credible interval. The color palettes of the GAMs have been used on the unsmoothed maps.

Changes in recruitment and loss rates. At the continental scale, the temporal change of recruitment rate per route was not different from zero (Fig. 3C, $\Delta r = 1.50 \times 10^{-6}$, $\mathrm{CI} = [-2.25 \times 10^{-5}; 2.63 \times 10^{-5}]$), suggesting that the net per capita recruitment has not changed at the continental scale since 1987. There was *ca.* 25% of the 1,033 routes with a significant positive Δr, and 25% with a significant negative Δr. Conversely, change in loss rate was significantly different from zero but extremely low (Fig. 3E, $\Delta l = 2.53 \times 10^{-5}$, $\mathrm{CI} = [1.72 \times 10^{-7}; 5.06 \times 10^{-5}]$), corresponding to an additional loss of 86 individuals per 100,000 birds over the entire time series period. The smoothed spatial patterns of Δr (Fig. 3D) and Δl (Fig. 3F) match the spatial patterns of Δg (Fig. 3B), with the Mid-Atlantic region (especially Delaware, Maryland, and New Jersey), the Midwest, and California having a combination of negative Δr and positive Δl. In other words, regions that underwent an increase in loss rate also saw a decrease in recruitment rate.

The main process of the acceleration of population declines: recruitment or loss rate change? Among the 505 routes with positive Δg, *ca.* 13% of them had significantly (i.e. considering the 95% credible interval of both Δr and Δl) a positive Δr as the primary component (Fig. 4A, green), while negative Δl accounted for 14% of them (Fig. 4A, blue). For the 528 routes with a negative Δg, 25% significantly showed a positive Δl as the main component (Fig. 4A, red), while it was a negative Δr for 15% of them (Fig. 4A, orange). Applying the spatial smoother revealed the demographic rates behind the negative Δg (*i.e.* behind the decrease of g in the Midwest, Mid-Atlantic, and California, Fig. 3B): Δl was the main component of the decrease in g across the Midwest and California (Fig. 4D, red), whereas Δr dominated across the Mid-Atlantic (Fig. 4D, orange).

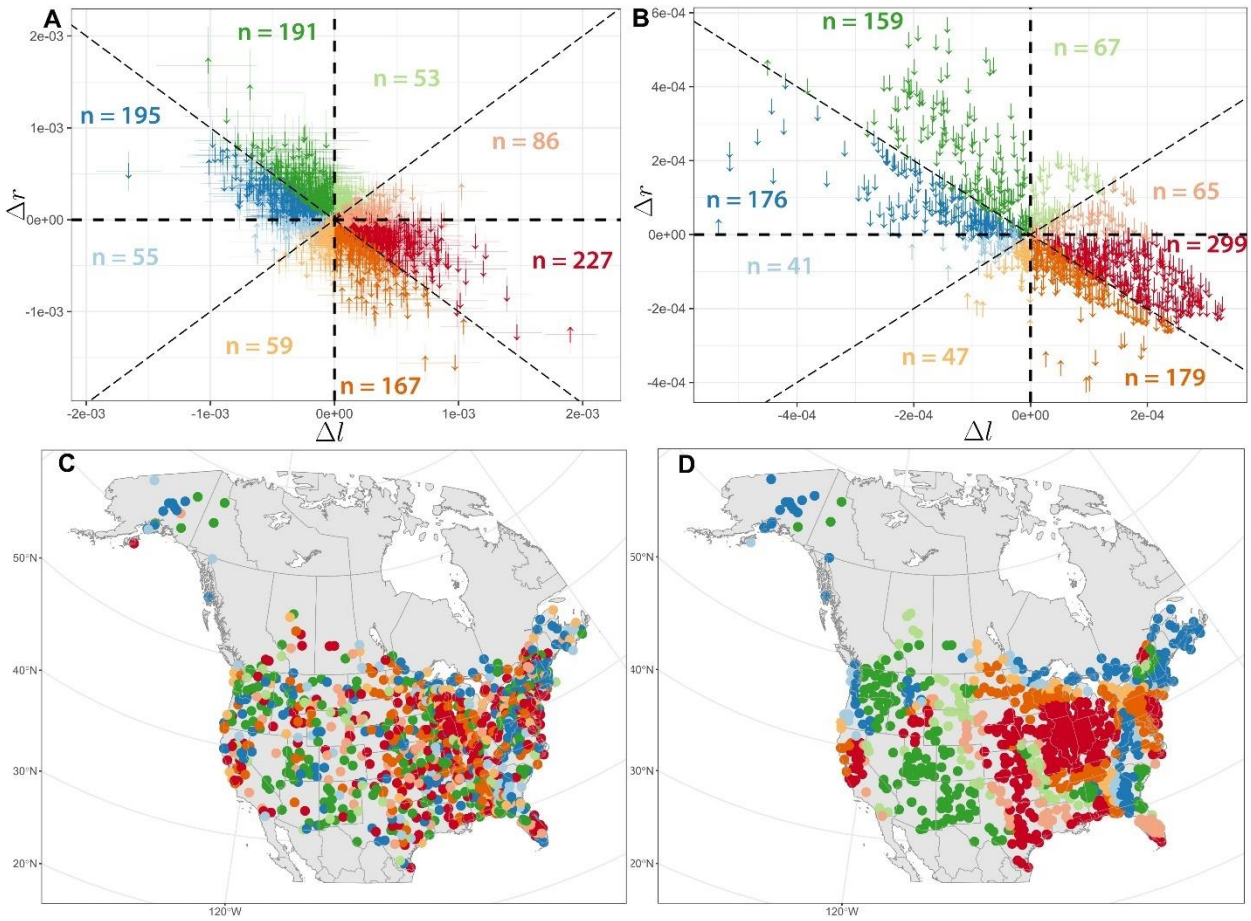

Fig. 4 | Eight classes of temporal change of vital rates. (A) Predicted and (B) spatially smoothed growth rate change (Δg) projected in a loss rate change (Δl) – recruitment rate change (Δr) space. Arrows (↑ and ↓) indicate abundance increases and declines, respectively, for each Breeding Bird Survey route. Colors represent whether the dominant process of Δg is due to negative Δl (blue), positive Δr (green), negative Δr (orange) or positive Δl (red) (see Fig. 1 for details). Error bars in (A) around each arrow represent the 95% credible interval for the grand Δl and grand Δr. Note that the scale in (B) is one order of magnitude smaller than in (A). (C) and (D) show spatial distribution of predicted and spatially smoothed values, respectively, with the smoothed map showing the main component of the acceleration in bird population decline. Colors indicate the dominant process: blue is dominant negative Δl, green is dominant positive Δr, orange is dominant negative Δr and, red is dominant positive Δl.

Per-species, per-family, and per-habitat analyses. We assessed Δg, Δr and Δl at different levels of taxonomic aggregation: species, family, and preferred habitat. Across 234 species, 66 showed positive ΔN (64 significant) of which 77% (51) had negative Δg (Fig. 5A, Fig. 5D, red and orange), with significantly dominating negative Δr (67%, 44, Fig. 5A, orange). Additionally, 21 out of 51 families had positive ΔN (14 significant), of which 95% (20) had negative Δg due to significantly negative Δr (Fig. 5D, orange). This indicates that the majority of species and families with increasing abundance are at the same time experiencing a decrease in growth rate, mainly attributed to a decline in recruitment rate, and are tending toward an eventual decline. Concerning the 168 species with negative ΔN, 52% (88) had a significant negative Δg, while only 4% (8) showed a significant positive Δg. This indicates that more than half of the species with declining abundance are undergoing an acceleration of this decline. Out of the 10 habitats, 4 habitats had a positive ΔN but only 2 significant (lakes/ponds and forests, Fig. 5C).

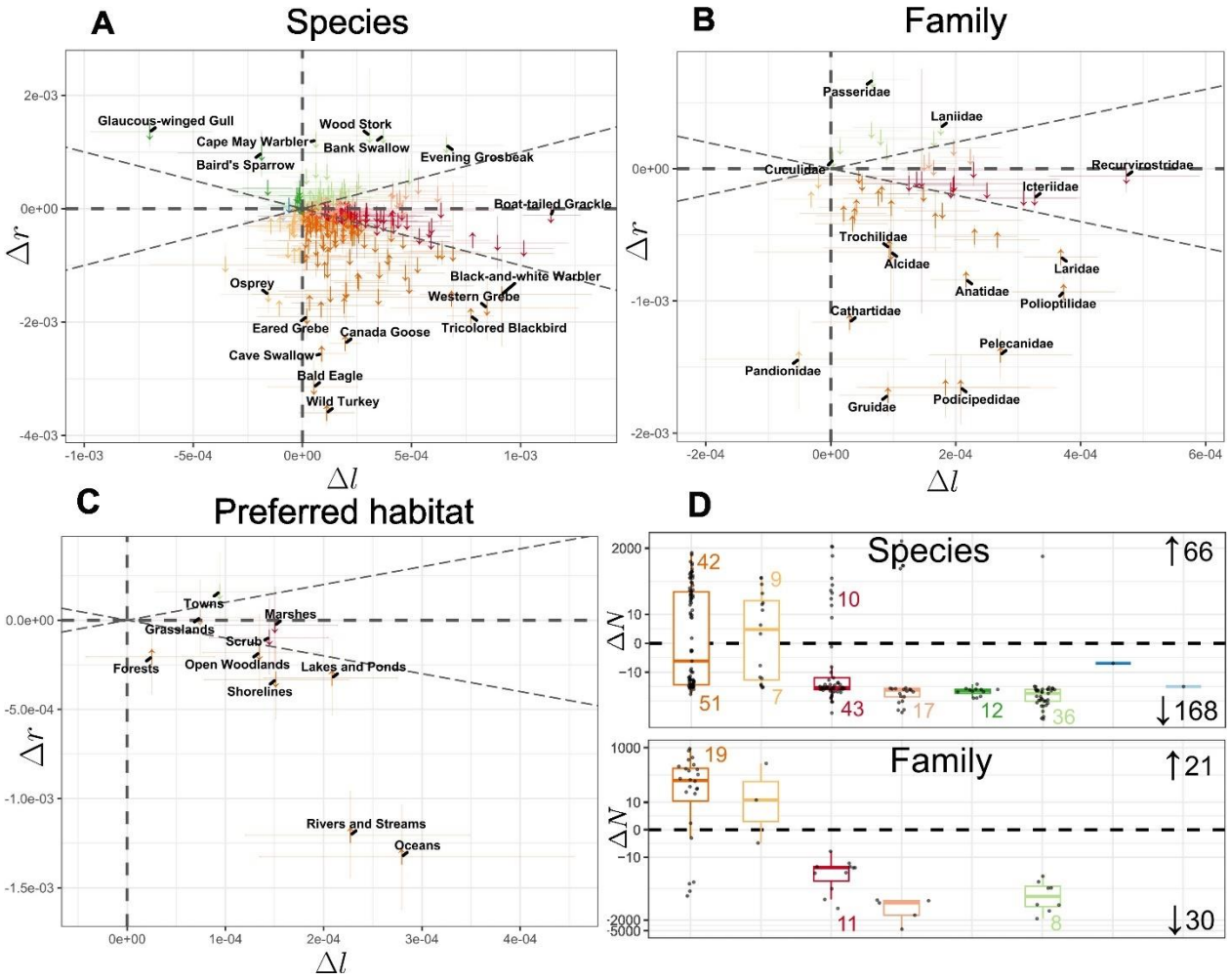

Fig. 5 | Temporal change of vital rates at different levels of taxonomic aggregation. Growth rate change (Δg) projected in a loss rate change (Δl) – recruitment rate change (Δr) space for (A) all 234 bird species, (B) 51 avian families, and (C) 10 preferred habitats. Arrows indicate abundance change (↑ positive and ↓ negative ΔN) for each species, family, and habitat. Error bars around each arrow represent the 95% credible interval for Δl and grand Δr. (D) Distributions of increasing and decreasing populations ΔN (above and below black dashed line, respectively) falling within each $\Delta l \Delta r$ class for bird species (top panel) and families (bottom panel). Colors indicate the dominant process: blue is dominant negative Δl, green is dominant positive Δr, orange is dominant negative Δr and, red is dominant positive Δl.

Discussion

Our findings corroborate the decline of bird abundance across North America [13] (Fig. 2) and align with trends seen for some European bird species [7,12,25–28]. Here, we extend this understanding by identifying specific regions where these declines are accelerating and by dissecting population dynamics into loss and recruitment rates.

Regional hotspots of accelerating bird population decline. We identify the Mid-Atlantic, the Midwest, and California as hotspots of accelerating decline of bird abundance (Fig. 3B). In these regions, the difference between the number of lost and recruited individuals continues to expand every year, raising concerns for the future of these bird populations. The decline of bird abundance has been associated with agricultural intensification [12,25,27,29,30] and changes in land-use [25,26]. Our findings align with this, as spatial patterns of accelerating decline (Fig. 3B) coincide with those of agriculture [31] and pesticide use (Pesticide National Synthesis Project, https://water.usgs.gov/nawqa/pnsp/usage/maps/), which have intensified in

North America [30]. The spatial hotspots of accelerating decline also align with patterns of human population density, particularly in the eastern USA and along the West Coast (U. S. Census Bureau, http://www.census.gov), and with CO2 emissions [32]. This suggests that regions experiencing strong human activities are also witnessing an acceleration in bird population decline, and that the decline of abundance *per se* does not necessarily directly correlate with human activities (Fig. 2) but patterns of accelerating decline do (Fig. 3B), although the direct causality remains to be tested in future studies. Acceleration of human impacts on ecosystems can lead to population collapse, as already observed for both terrestrial [33,34] and marine ecosystems [35–37]. This is concerning, especially in the context of the ongoing Great Acceleration [17,18], where global human activities are accelerating due to economic growth aspirations [15]. Our results serve as a warning that a similar collapse could unfold among the bird populations of North America.

Is recruitment or loss the main component of the acceleration of bird population decline? We further demonstrate how changes in loss and recruitment rates contribute to the acceleration of bird population decline (Fig. 3E-F, Fig. 4). Loss of individuals is frequently linked to pollution [38,39], extreme events induced by climate change [40], disease outbreaks [41,42] or human disturbances [43,44]. In contrast, recruitment rate is directly linked to breeding success determined by the clutch size and successful fledges, and is driven by precipitation, habitat fragmentation, availability of nesting sites or food [45,46]. Admittedly, extreme events, climatic fluctuations, disease outbreaks, and changes in land-use can impact both recruitment and loss of individuals, albeit with different relative magnitude. While we have not disentangled the relative importance of those drivers for the reported population declines and demographic rates, our results offer a foundation for both future experimental studies and conservation policies.

Decline in recruitment rates. Importantly, we have revealed that 67% of species and 95% of families with increasing abundance are undergoing a decline in recruitment rates (Fig. 5D). This suggests that most of the taxa with increasing abundance are, in fact, heading towards an eventual decline, should such a trend continue. However, we warn that our models didn't account for density-dependence and that this pattern of decreasing recruitment rate for increasing population might be due to some species reaching their carrying capacity; an opportunity for future analysis, e.g. as in ref. [48]. Decrease in recruitment rate has been linked to habitat fragmentation [49] or decrease in food abundance [50,51], both of which have intensified since 1987 [52]. Importantly, decrease in bird abundance is often seen as a direct result of the loss of individuals, and conservation policies often aim at directly reducing this loss. We show, however, that decreases in recruitment rate may themselves be responsible for significant population dynamics, stressing the importance of prioritizing increasing bird recruitment on par with preventing the loss. For instance, a decrease in the use of neonicotinoids [27,53] or installation of nest boxes [54] are policies supporting recruitment, with a potential to bend the curve of a future recruitment collapse.

Using one of the most comprehensive local bird time series datasets in the world, coupled with a model disentangling processes of recruitment and loss, we provide insights into the abundance dynamics and their underlying processes of 234 species over 35 years across a continental scale. This marks a significant advancement, as we offer detailed insights into demographic dynamics that were previously unexplored for such a broad spectrum of species and at such an expansive spatial scale. Importantly, we reveal geographic hotspots of acceleration of bird abundance decline and attribute these declines to shifts of recruitment and loss since 1987. We propose that regions with accelerated decline correspond to areas with high human populations and activities, which are themselves increasing at an accelerated pace. We also highlight a concerning trend: most of the species with an increasing population is trending toward an eventual decline due to a ubiquitous decrease in recruitment rate. This is alarming, especially considering projections of exponential acceleration in human activities across various sectors such as economy, agriculture, or transportation, with no foreseeable reversal of this trend.

Methods

Data. To investigate the acceleration of bird decline in North America, we used the North American Breeding Bird Survey [24], an ongoing bird monitoring initiative launched in 1966. Spanning more than 50 years, the BBS comprises 39.2 km-long routes scattered across the contiguous United States and Canada, each divided into 50 census points at approximately 800 m intervals. From its inception with about 500 routes in 1966, the BBS has grown to encompass 5,581 routes by 2021. At the time of our data download on September 5, 2022, the data contained 6,946,871 records of species abundances compiled by 10,316 volunteers for 746 species and spanning over 50 years. The BBS data also contain meteorological data, date, hour, and spatial coordinates.

Routes with long time-series (*e.g.* from 1969 to 2021) were spatially sparse. To balance long temporal extent with robust spatial coverage, we focused our analysis on the 1987-2021 period and selected routes with no more than 15 years of missing data.

For each species, we extracted the preferred habitat from the eBird/Cornell online database [24]. These were: Towns, Grasslands, Shorelines, Scrubs, Deserts, Rivers and Streams, Marshes, Open Woodlands, Forests, Lakes and Ponds, Oceans, and Tundra. Species with missing habitat data (23 in total) were excluded. In the end, we performed our analysis using 1,033 routes from 1987 to 2021 (*i.e.* 35 years), with 1,623,394 occurrences of 564 species.

Dynamic *N*-mixture model. We modelled the abundance of each of the 564 bird species across each route and year from 1987 to 2021 using a dynamic *N*-mixture model (Dail & Madsen, 2011), hereafter the DM model. It is a generalization of the *N*-mixture model by Royle (2004) that assumes open populations (*i.e.* metapopulations can experience births, recruitments, deaths, or emigrations) and that has been successfully applied to the BBS [22,23]. This model can also be used without repeated counts [23].

For a species j and a route i, the abundance at time $t+1$ (*i.e.* $N_{j,i,t+1}$) is the sum of surviving ($S_{j,i,t+1}$) and recruited ($R_{j,i,t+1}$) individuals from time t:

$$N_{j,i,t+1} = S_{j,i,t+1} + R_{j,i,t+1} \qquad \text{eq. 1}$$

with survival $S_{j,i,t+1}$ and recruitment $R_{j,i,t+1}$ modelled as:

$$S_{j,i,t+1} \sim Binomial(N_{j,i,t}, \phi_{j,i,t}) \qquad \text{eq. 2}$$

$$R_{j,i,t+1} \sim Poisson(\gamma_{j,i,t}) \qquad \text{eq. 3}$$

$N_{j,i,t}$ is the abundance of species j at route i and time t, ϕ is the average probability of individual survival, and γ is the number of recruited individuals. The abundance at time 1 ($N_{j,i,1}$) is:

$$N_{j,i,1} \sim Poisson(\lambda_{j,i,1}), \text{eq. 4}$$

where λ is the mean abundance of the species at time 1.

The DM model corrects for imperfect detection, where the *observed* abundance ($n_{j,i,t}$) is corrected to estimate the true abundance ($N_{j,i,t}$):

$$n_{(j,i,t)} \sim Binomial\left(N_{j,i,t}, p_{j,i,t}\right) \text{eq. 5}$$

$$\text{logit}\left(p_{j,i,t}\right) = \alpha + \boldsymbol{x}_{j,i,t}^{\intercal}\boldsymbol{b}, \qquad \text{eq. 6}$$

where p is the probability of detection of an individual, $\boldsymbol{x}^{\intercal}$ is the transpose of a vector of covariates, $\boldsymbol{b}$ is a vector of regression coefficients, and α is the intercept. $\boldsymbol{x}$ includes the exact time of the day of the census (in decimal hours), and weather data, *i.e.* wind condition (ordinal variable with 9 levels ranging from < 2 km.h^{-1} to 74 km.h^{-1}), sky condition (factor with 7 levels: clear sky, partly cloudy, cloudy, fog, drizzle, snow, and shower), and average temperature during the census (in °C). Missing values for the time of the day and temperature were imputed following Kéry and Royle (2015):

$$x_{i,t} \sim Normal(\mu, \sigma) \qquad \text{eq. 7}$$

where $x_{i,t}$ is the imputed value of the covariate x at route i and time t, and μ and σ are means and standard deviation of the available data.

For each *j*-th species, we fitted the DM model in a Bayesian framework using MCMC sampler JAGS (Plummer, 2003; https://mcmc-jags.sourceforge.io/), interfaced through the package jagsUI [58] in R ver. 4.2.1 [59]. For all the parameters, we used normal distributions with 0 mean and variance of 100 (Appendix B). The settings for the MCMC algorithm were: 3 chains, 100,000 iterations per chain, 75,000 burn-in, a thinning rate of 10, and 1,000 iterations in the adaptative phase. The entire fitting procedure for all 564 species (1 core per MCMC chain, 3 chains per species) required *ca.* 2 days on 1,692 cores of the Ohio Supercomputer (https://www.osc.edu/), each core operating at 2.5 GHz.

For each species, the DM models' convergence was assessed by computing the $\hat{R}$ (Rhat, Gelman & Rubin, 1992) for all of the 106,419 monitored values. To select the most trustful models, we selected those with median $\hat{R} \leq 1.1$. This led to a final set of 234 species for further analysis.

Rates of change. From the output of the DM model and for each *j*-th species at *i*-th site and *t*-th year (starting from 1988), we derived the yearly number of lost individuals L, as well as the per-capita growth rate g, per-capita recruitment rate r, and per-capita loss rate l:

$$L_{j,i,t+1} = N_{j,i,t} - S_{j,i,t+1} \qquad \text{eq. 8}$$

$$g_{j,i,t+1} = \frac{N_{j,i,t+1} - N_{j,i,t}}{N_{j,i,t}} = \frac{\Delta N}{N_t} \qquad \text{eq. 9}$$

$$r_{j,i,t+1} = \frac{R_{j,i,t+1}}{N_{j,i,t}} \qquad \text{eq. 10}$$

$$l_{j,i,t+1} = \frac{L_{j,i,t+1}}{N_{j,i,t}} \qquad \text{eq. 11}$$

Additionally, we calculated the per-capita growth rate relative to the size of the initial population in 1987, hereafter relative growth rate g_{t1}, as:

$$g_{t1\,|\,j,i,t} = \frac{N_{j,i,t} - N_{j,i,1}}{N_{j,i,1}} \qquad \text{eq. 12}$$

Per route, per species, per family and per habitat analyses. We assessed all metrics for different levels of aggregation. First, for each route, we aggregated the number of individuals, recruitments, or losses of all the species together and assessed these aggregated rates. Conversely, for each species, family or preferred habitat, we aggregated those metrics over all the routes. In other words, these were not mapped geographically as in the spatial analysis, but the numbers were aggregated for each grouping (species, family, habitat) over all 1,033 routes included in our analysis.

In the DM model, each value of $N_{j,i,t}$, $S_{j,i,t}$, $R_{j,i,t}$ (and thus $L_{j,i,t}$) for each species j, site i, and time t is estimated with a posterior distribution. To propagate the uncertainty of these estimates to the higher levels

of aggregations (namely route, family and preferred habitat), we sampled each of those posterior distributions 500 times. For each sample, we aggregated those values per route, family or preferred habitat. This gave us a new posterior distribution of N, R and L with a mean ($y_{j,t}$) and standard deviation ($sd_{j,t}$) at the desired level of aggregation. We performed the same propagation of uncertainty for the rates g_{t1}, g, r, and l across all the levels of aggregation.

Temporal change with Bayesian mixed models. We assessed the temporal change of the estimated N, g, r, and l for the different levels of aggregation while propagating the uncertainty of these estimates from the posteriors of the DM model, using mixed models. We used a random varying slope and intercept for each route, species, family or preferred habitat:

$$y_{j,t} = \Delta y_j \times t + \beta_{0_j} + \epsilon_{j,t}, \qquad \text{eq. 13}$$

where $y_{j,t}$ is the mean of the posterior distribution (see previous paragraph) estimated by the DM model, Δy_j and β_{0_j} are the random slopes and intercepts, j is the index of the level of aggregation (e.g. j-th route) and t the year in the time series. The error term $\epsilon_{j,t}$ comes from a normal distribution

$$\epsilon_{j,t} \sim N(0, sd_{j,t}), \qquad \text{eq. 14}$$

where $sd_{\mathrm{j,t}}$ is the standard deviation of the posterior distribution of $y_{j,t}$ estimated in the DM model (see previous paragraph). This way, the uncertainty of all the y metrics (estimated in the DM model) is propagated to the mixed effect model of temporal trends, an approach used in meta analyses [61]. Finally, the random slopes Δy_j and intercepts β_{0_j} come from normal distributions:

$$\Delta y_j \sim N(\mathrm{M}_{\Delta \mathrm{y}}, \mathrm{SD}_{\Delta \mathrm{y}}) \quad \text{eq. 15}$$

$$\beta_{0_j} \sim N(M_{\beta_0}, SD_{\beta_0}) \quad \text{eq. 16}$$

The posterior distributions of $\mathrm{M}_{\Delta \mathrm{y}}$ and M_{β_0}represent the grand means of the trends and describe the overall temporal trend across all *j*s.

Spatial smoothing. For the spatial analysis, mapping the above-mentioned temporal changes (ΔN, Δg_{t1}, $\Delta g, \Delta l, \Delta r$) may reveal a substantial local variation among individual routes, which could obscure average trends across larger regions. To detect these regional anomalies, we smoothed the variation of the rates using spatial generalized additive models (GAM) using the R package mgcv [62]:

$$\Delta y_j = \mathrm{s}(Lon_j, Lat_j), \quad \text{eq. 17}$$

with Δy_j the temporal change of the metric considered at route j, Lon and Lat the longitude and latitude of the route j, and $s()$ indicating that longitude and latitude are treated as interacting covariates in the spline function of the smoother. For the spline function, we used a gaussian process as a smooth class (argument "bs" of the $s()$ function in mgcv) with 100 basis functions (*ca.* $\frac{1}{10}^{th}$ of the number of routes).

Classification of acceleration and deceleration. The same Δg value can emerge from different combinations of Δl and Δr; that is, acceleration or deceleration of ΔN can result from increases or decreases in per-capita loss, recruitment, or both. To capture this complexity, we devised a classification system for temporal population dynamics based on Δl and Δr (Fig. 1b, c), which allowed us to show the relative importance of Δl and Δr in a single map. We created a color scheme where each route (or species, family, or preferred habitat) lays in a 2-dimensional space with Δl on the x-axis and Δr on the y-axis (henceforth $\Delta l \Delta r$ space). For instance, our analysis reveals that at the route level, the average ΔN is

negative (indicated by ↓). In this case, blue and green hues indicate deceleration of population decline (Fig. 1C), which can be mainly attributed to either a negative Δl (blue) or to a positive Δr (green). Conversely, still in the case of a negative ΔN (↓), red and orange hues indicate an acceleration of the decline, and that either a positive Δl (red) or a negative Δr (orange) is the main component of the acceleration. This classification was applied to individual routes, as well as to smoothed averages. We note that for positive ΔN (indicate by ↑), implications of the color scheme are slightly different (*i.e.* either acceleration or deceleration of increasing population), but the interpretation about positive or negative Δr and Δl remains consistent.

References

1. IPBES. Global Assessment Report on Biodiversity and Ecosystem Services of the Intergovernmental Science-Policy Platform on Biodiversity and Ecosystem Services. https://zenodo.org/record/3831673 (2019) doi:10.5281/ZENODO.3831673.
2. Callaghan, C. T., Santini, L., Spake, R. & Bowler, D. E. Population abundance estimates in conservation and biodiversity research. Trends in Ecology & Evolution **39**, 515–523 (2024).
3. Leung, B. et al. Clustered versus catastrophic global vertebrate declines. Nature **588**, 267–271 (2020).
4. Toszogyova, A., Smycka, J. & Storch, D. Mathematical biases in the calculation of the Living Planet Index lead to overestimation of vertebrate population decline. Preprint at https://doi.org/10.21203/rs.3.rs-2887653/v1 (2023).
5. Daskalova, G. N., Myers-Smith, I. H. & Godlee, J. L. Rare and common vertebrates span a wide spectrum of population trends. Nat Commun **11**, 4394 (2020).
6. Dornelas, M. et al. Looking back on biodiversity change: lessons for the road ahead. Philosophical Transactions of the Royal Society B: Biological Sciences **378**, 20220199 (2023).
7. Inger, R. et al. Common European birds are declining rapidly while less abundant species' numbers are rising. Ecology Letters **18**, 28–36 (2015).
8. Leung, B., Greenberg, D. A. & Green, D. M. Trends in mean growth and stability in temperate vertebrate populations. Diversity and Distributions **23**, 1372–1380 (2017).
9. Pilotto, F. et al. Meta-analysis of multidecadal biodiversity trends in Europe. Nat Commun **11**, 3486 (2020).
10. Van Klink, R. et al. Meta-analysis reveals declines in terrestrial but increases in freshwater insect abundances. Science **368**, 417–420 (2020).
11. Johnson, T. F. et al. Revealing uncertainty in the status of biodiversity change. Nature (2024) doi:10.1038/s41586-024-07236-z.
12. Rigal, S. et al. Farmland practices are driving bird population decline across Europe. Proceedings of the National Academy of Sciences **120**, e2216573120 (2023).
13. Rosenberg, K. V. et al. Decline of the North American avifauna. Science **366**, 120–124 (2019).
14. Díaz, S. et al. Pervasive human-driven decline of life on Earth points to the need for transformative change. Science **366**, eaax3100 (2019).
15. Meadows, D. H., Randers, J. & Meadows, D. L. The Limits to Growth (1972). in The Future of Nature (eds. Robin, L., Sörlin, S. & Warde, P.) 101–116 (Yale University Press, 2017). doi:10.12987/9780300188479-012.
16. Piketty, T. Capital in the Twenty-First Century. (Harvard University Press, 2014). doi:10.4159/9780674369542.
17. 7. Land Use and the Great Acceleration in Human Activities: Political and Economic Dynamics. in The Sociology of Development Handbook (ed. Hooks, G.) 190–206 (University of California Press, 2019). doi:10.1525/9780520963474-009.
18. Steffen, W., Broadgate, W., Deutsch, L., Gaffney, O. & Ludwig, C. The trajectory of the Anthropocene: The Great Acceleration. The Anthropocene Review **2**, 81–98 (2015).
19. Barnosky, A. D. et al. Has the Earth's sixth mass extinction already arrived? Nature **471**, 51–57 (2011).

20. Ceballos, G. et al. Accelerated modern human–induced species losses: Entering the sixth mass extinction. Sci. Adv. **1**, e1400253 (2015).
21. Urban, M. C. Accelerating extinction risk from climate change. Science **348**, 571–573 (2015).
22. Dail, D. & Madsen, L. Models for Estimating Abundance from Repeated Counts of an Open Metapopulation. Biometrics **67**, 577–587 (2011).
23. Kéry, M. & Royle, J. A. Applied Hierarchical Modeling in Ecology: Analysis of Distribution, Abundance and Species Richness in R and BUGS: Volume 2: Dynamic and Advanced Models. (Academic Press, Cambridge, 2020).
24. Ziolkowski Jr., D., Lutmerding, M., Aponte, V. & Hudson, M.-A. 2022 Release - North American Breeding Bird Survey Dataset (1966-2021). U.S. Geological Survey https://doi.org/10.5066/P97WAZE5 (2022).
25. Bowler, D. E., Heldbjerg, H., Fox, A. D., De Jong, M. & Böhning-Gaese, K. Long-term declines of European insectivorous bird populations and potential causes. Conservation Biology **33**, 1120–1130 (2019).
26. Fraixedas, S. et al. Substantial decline of Northern European peatland bird populations: Consequences of drainage. Biological Conservation **214**, 223–232 (2017).
27. Hallmann, C. A., Foppen, R. P. B., Van Turnhout, C. A. M., De Kroon, H. & Jongejans, E. Declines in insectivorous birds are associated with high neonicotinoid concentrations. Nature **511**, 341–343 (2014).
28. Newton, I. The recent declines of farmland bird populations in Britain: an appraisal of causal factors and conservation actions. Ibis **146**, 579–600 (2004).
29. Green, R. E., Cornell, S. J., Scharlemann, J. P. W. & Balmford, A. Farming and the Fate of Wild Nature. Science **307**, 550–555 (2005).
30. Stanton, R. L., Morrissey, C. A. & Clark, R. G. Analysis of trends and agricultural drivers of farmland bird declines in North America: A review. Agriculture, Ecosystems & Environment **254**, 244–254 (2018).
31. Yan, L. & Roy, D. P. Conterminous United States crop field size quantification from multi-temporal Landsat data. Remote Sensing of Environment **172**, 67–86 (2016).
32. Gurney, K. R. et al. The Vulcan Version 3.0 High-Resolution Fossil Fuel CO_2 Emissions for the United States. JGR Atmospheres **125**, e2020JD032974 (2020).
33. Newbold, T., Tittensor, D. P., Harfoot, M. B. J., Scharlemann, J. P. W. & Purves, D. W. Non-linear changes in modelled terrestrial ecosystems subjected to perturbations. Sci Rep **10**, 14051 (2020).
34. Reid, N. et al. Regime shift tipping point in hare population collapse associated with climatic and agricultural change during the very early 20th century. Global Change Biology **27**, 3732–3740 (2021).
35. Chen, H., Hagerty, S., Crotty, S. M. & Bertness, M. D. Direct and indirect trophic effects of predator depletion on basal trophic levels. Ecology **97**, 338–346 (2016).
36. Frank, K. T., Petrie, B., Choi, J. S. & Leggett, W. C. Trophic Cascades in a Formerly Cod-Dominated Ecosystem. Science **308**, 1621–1623 (2005).
37. Jackson, J. B. C. et al. Historical Overfishing and the Recent Collapse of Coastal Ecosystems. Science **293**, 629–637 (2001).
38. La Sorte, F. A., Lepczyk, C. A. & Aronson, M. F. J. Light pollution enhances ground-level exposure to airborne toxic chemicals for nocturnally migrating passerines. Global Change Biology **29**, 57–68 (2023).
39. Liang, Y. et al. Conservation cobenefits from air pollution regulation: Evidence from birds. Proc. Natl. Acad. Sci. U.S.A. **117**, 30900–30906 (2020).
40. Burthe, S., Wanless, S., Newell, M., Butler, A. & Daunt, F. Assessing the vulnerability of the marine bird community in the western North Sea to climate change and other anthropogenic impacts. Mar. Ecol. Prog. Ser. **507**, 277–295 (2014).
41. Chavatte, J.-M. et al. An outbreak of trichomonosis in European greenfinches Chloris chloris and European goldfinches Carduelis carduelis wintering in Northern France. Parasite **26**, 21 (2019).

42. Lühken, R. et al. Distribution of Usutu Virus in Germany and Its Effect on Breeding Bird Populations. Emerg. Infect. Dis. **23**, 1994–2001 (2017).
43. Fahrig, L. & Rytwinski, T. Effects of Roads on Animal Abundance: an Empirical Review and Synthesis. E&S **14**, art21 (2009).
44. Tryjanowski, P. et al. Urban and rural habitats differ in number and type of bird feeders and in bird species consuming supplementary food. Environ Sci Pollut Res **22**, 15097–15103 (2015).
45. Bennett, J. M., Clarke, R. H., Thomson, J. R. & Mac Nally, R. Fragmentation, vegetation change and irruptive competitors affect recruitment of woodland birds. Ecography **38**, 163–171 (2015).
46. Cam, E. & Aubry, L. Early development, recruitment and life history trajectory in long-lived birds. J Ornithol **152**, 187–201 (2011).
47. Freckleton, R. P. Dealing with collinearity in behavioural and ecological data: model averaging and the problems of measurement error. Behav Ecol Sociobiol **65**, 91–101 (2011).
48. Bellier, E., Kéry, M. & Schaub, M. Simulation-based assessment of dynamic N -mixture models in the presence of density dependence and environmental stochasticity. Methods Ecol Evol **7**, 1029–1040 (2016).
49. Robinson, S. K., Thompson, F. R., Donovan, T. M., Whitehead, D. R. & Faaborg, J. Regional Forest Fragmentation and the Nesting Success of Migratory Birds. Science **267**, 1987–1990 (1995).
50. Holmes, R. T. & Sherry, T. W. Thirty-Year Bird Population Trends in an Unfragmented Temperate Deciduous Forest: Importance of Habitat Change. The Auk **118**, 589–609 (2001).
51. Ponce, C., Bravo, C. & Alonso, J. C. Effects of agri-environmental schemes on farmland birds: do food availability measurements improve patterns obtained from simple habitat models? Ecology and Evolution **4**, 2834–2847 (2014).
52. Alofs, K. M. & Fowler, N. L. Habitat fragmentation caused by woody plant encroachment inhibits the spread of an invasive grass. Journal of Applied Ecology **47**, 338–347 (2010).
53. Li, Y., Miao, R. & Khanna, M. Neonicotinoids and decline in bird biodiversity in the United States. Nat Sustain **3**, 1027–1035 (2020).
54. Møller, A. P. et al. Clutch-size variation in Western Palaearctic secondary hole-nesting passerine birds in relation to nest box design. Methods Ecol Evol **5**, 353–362 (2014).
55. Royle, J. A. N-Mixture Models for Estimating Population Size from Spatially Replicated Counts. Biometrics **60**, 108–115 (2004).
56. Kéry, M. & Royle, J. A. Applied Hierarchical Modeling in Ecology: Analysis of Distribution, Abundance and Species Richness in R and BUGS: Volume 1:Prelude and Static Models. (Academic Press, Amsterdam ; Boston, 2015).
57. Plummer, M. JAGS: A program for analysis of Bayesian graphical models using Gibbs sampling. In K. Hornik, F. Leisch, & A. Zeileis (Eds.), Proceedings of the 3rd International Workshop on Distributed Statistical Computing, 124(125.10), 1–10. (2003).
58. Kellner, K. jagsUI: A Wrapper Around 'rjags' to Streamline 'JAGS' Analyses. (2021).
59. R Core Team. R: A Language and Environment for Statistical Computing. (R Foundation for Statistical Computing, Vienna, Austria, 2021).
60. Gelman, A. & Rubin, D. B. Inference from Iterative Simulation Using Multiple Sequences. Statist. Sci. **7**, (1992).
61. Viechtbauer, W. Conducting Meta-Analyses in R with the **metafor** Package. J. Stat. Soft. **36**, (2010).
62. Wood, S. N. Fast stable restricted maximum likelihood and marginal likelihood estimation of semiparametric generalized linear models. Journal of the Royal Statistical Society (B) **73**, 3–36 (2011).

Supplementary information.

Appendix A: Figs. S1 to S2

Appendix B: JAGS code of the Dail-Madsen model

Data, scripts, and figures are available on the following GitHub repository: https://github.com/FrsLry/ms_acceleration.

Acknowledgements. This study stands on the shoulders of the thousands of volunteers who participated in the North American BBS, and the institutions that manage this program. F.L. and P.K. were funded by the European Union (ERC, BEAST, 101044740). Views and opinions expressed are however those of the author(s) only and do not necessarily reflect those of the European Union or the European Research Council Executive Agency. Neither the European Union nor the granting authority can be held responsible for them. M.A.J. was supported by the National Science Foundation DEB-1926598. The authors thank the Ohio Supercomputer Center for their computational resources. We thank three anonymous reviewers for their helpful comments.

Author Contributions. F.L. performed the statistical analysis. F.L, M.J., and P.K. wrote the paper.

Competing interest. The authors declare no competing financial interests.

Author information. Correspondence and requests for materials should be addressed to F.L. (leroy@fzp.czu.cz).

Appendix A

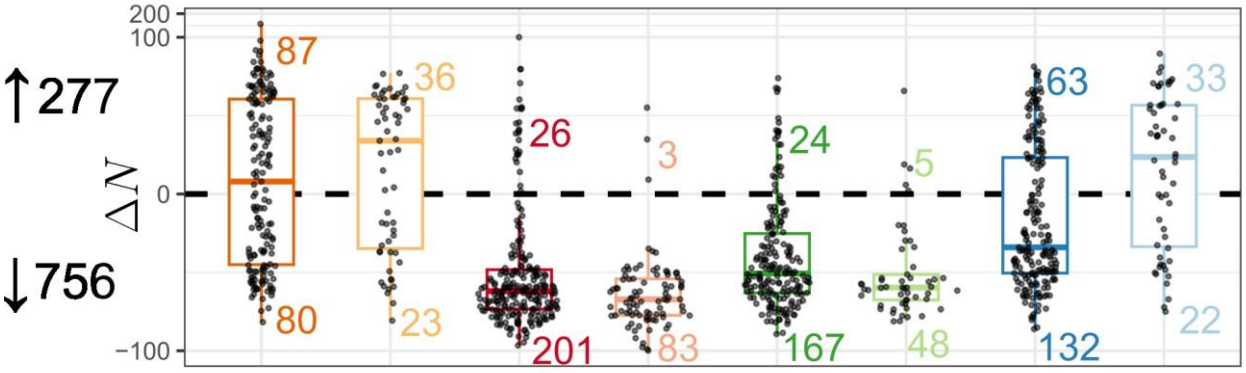

Appendix A Fig. 1: Distributions of increasing and decreasing populations ΔN (above and below black dashed line, respectively) falling within each $\Delta l \Delta r$ class for the 1033 BBS routes in our analysis. Colors indicate the dominant process: blue is dominant negative Δl, green is dominant positive Δr, orange is dominant negative Δr and, red is dominant positive Δl. The arrows on the right indicate the number of routes with positive and negative ΔN.

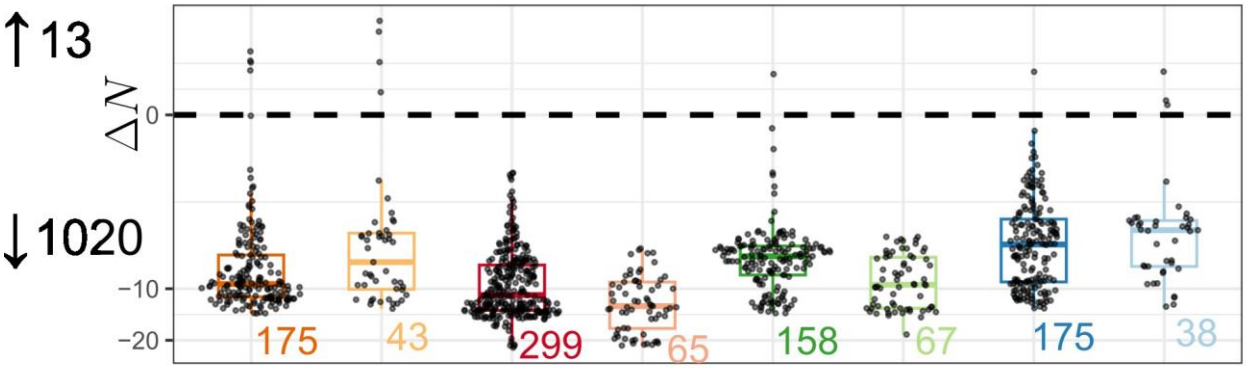

Appendix A Fig. 2: Distributions of increasing and decreasing populations ΔN (above and below black dashed line, respectively) smoothed with GAM, falling within each $\Delta l \Delta r$ class for the 1033 BBS routes in our analysis. Colors indicate the dominant process: blue is dominant negative Δl, green is dominant positive Δr, orange is dominant negative Δr and, red is dominant positive Δl. The arrows on the right indicate the number of routes with positive and negative ΔN.

This file contains the JAGS code implementing the Dail-Madsen model, modified from Kéry & Royle (2020). The output of the model gives the abundance (N), as well as the number of surviving (S) and recruited (R) individuals. The code is commented to provide information about the parameters estimated.

```
model {
  # Priors
  alpha.lambda ~ dnorm(0,0.01)  ## lambda is the abundance at time 1
  alpha.gamma ~ dnorm(0,0.01)           ## gamma is the number of recruited individuals
  alpha.phi ~ dnorm(0,0.01)               ## phi is the probability of survival
  alpha.p ~ dnorm(0,0.01)                   ## p is the probability of detecting an individual (observation process)

  ### Priors Covariates #########           ## The following covariates were used in the detection probability of the observation
process
  beta.time ~ dnorm(0,0.01)                    ## time is the time of the day of the census
  beta.temp ~ dnorm(0,0.01)                    ## temp is the average temperature of the census
  ### Sky ###                                            ## sky indicates the discrete states of the sky conditions
  beta.sky[1] <- 0                                  ## 1 = Clear or few clouds
  beta.sky[2] ~ dnorm(0,0.01)                 ## 2 = Partly cloudy (scattered) or variable sky
  beta.sky[3] ~ dnorm(0,0.01)                 ## 3 = Cloudy (broken) or overcast
  beta.sky[4] ~ dnorm(0,0.01)                 ## 4 = Fog or smoke
  beta.sky[5] ~ dnorm(0,0.01)                 ## 5 = Drizzle
  beta.sky[6] ~ dnorm(0,0.01)         ## 6 = Snow
  beta.sky[7] ~ dnorm(0,0.01)         ## 7 = Showers
  ### Wind ###                        ## wind indicates the strength of the wind during the census
  beta.wind[1] <- 0                   ## 1 = Smoke rises vertically [<1 mph, <2 kph]
  beta.wind[2] ~ dnorm(0,0.01)        ## 2 = Wind direction shown by smoke drift [1-3 mph, 2-5 kph]
  beta.wind[3] ~ dnorm(0,0.01)        ## 3 = Wind felt on face; leaves rustle [4-7 mph, 6-12 kph]
  beta.wind[4] ~ dnorm(0,0.01)        ## 4 = Leaves, small twigs in constant motion [8-12 mph, 13-19 kph]
  beta.wind[5] ~ dnorm(0,0.01)        ## 5 = Dust rises; small branches move [13-18 mph, 20-29 Kph]
  beta.wind[6] ~ dnorm(0,0.01)        ## 6 = Small trees in leaf begin to sway [19-24 mph, 30-39 Kph]
  beta.wind[7] ~ dnorm(0,0.01)        ## 7 = Strong Breeze; Larger tree branches moving [25-31 mph, 40-50 kph]

  # Likelihood

  for(i in 1:nsites){

    # State process: initial condition
    N[i,1] ~ dpois(lambda[i,1])         ## Estimation of abundance at time 1
    for(t in 1:nyears){
    log(lambda[i,t]) <- alpha.lambda
    log(gamma[i,t])  <- alpha.gamma
    logit(phi[i,t])  <- alpha.phi
    }

    # State process: transition model   ## Estimation of Survival and Recruitment
    for(t in 1:(nyears-1)){
      S[i,t+1] ~ dbin(phi[i,t], N[i,t])
      R[i, t+1] ~ dpois(gamma[i,t])
```

```
        N[i,t+1] <- S[i,t+1] + R[i,t+1]
      }

      # Observation process               ## Correcting the observed abundance with a probability detection depending on covariates
      for(t in 1:nyears){
      logit(p[i,t]) <- alpha.p + beta.wind[wind[i,t]] + beta.sky[sky[i,t]] + beta.temp*temperature[i,t] + beta.time*time[i,t]

      C[i,t] ~ dbin(p[i,t], N[i,t])       ## C is the input data, or observed abundance
      }
    }

    # Covariate mean as a model for missing covariates
    for(i in 1:nsites){
      for(t in 1:nyears){
        time[i,t] ~ dnorm(mu.time, tau.time)
        temperature[i,t] ~ dnorm(mu.temp, tau.temp)
      }
    }

    # Priors for covariate mean as a model for missing covariates
    mu.time ~ dnorm(0, 0.0001)
    tau.time <- pow(sd.time, -2)
    sd.time ~ dunif(0, 100)
    mu.temp ~ dnorm(0, 0.0001)
    tau.temp <- pow(sd.temp, -2)
    sd.temp ~ dunif(0, 100)

  }
```

A

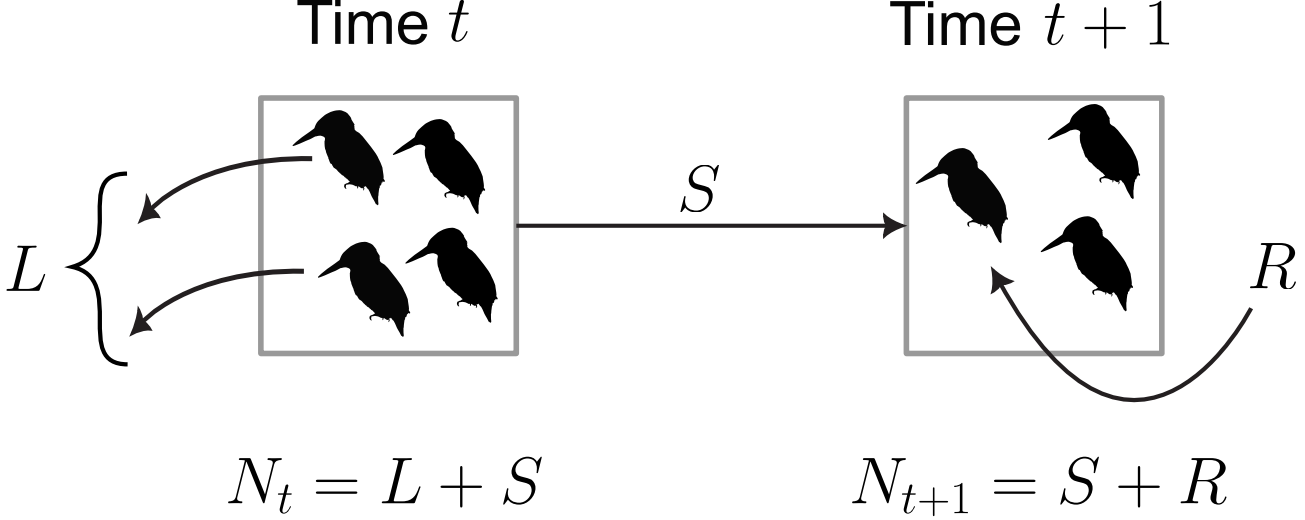

$$\Delta N = N_{t+1} - N_t = R - L$$

$$g = \frac{\Delta N}{N_t} = \frac{R}{N_t} - \frac{L}{N_t} = r - l$$

$$\Delta g = \Delta r - \Delta l = \Delta(\frac{\Delta N}{N_t})$$

B

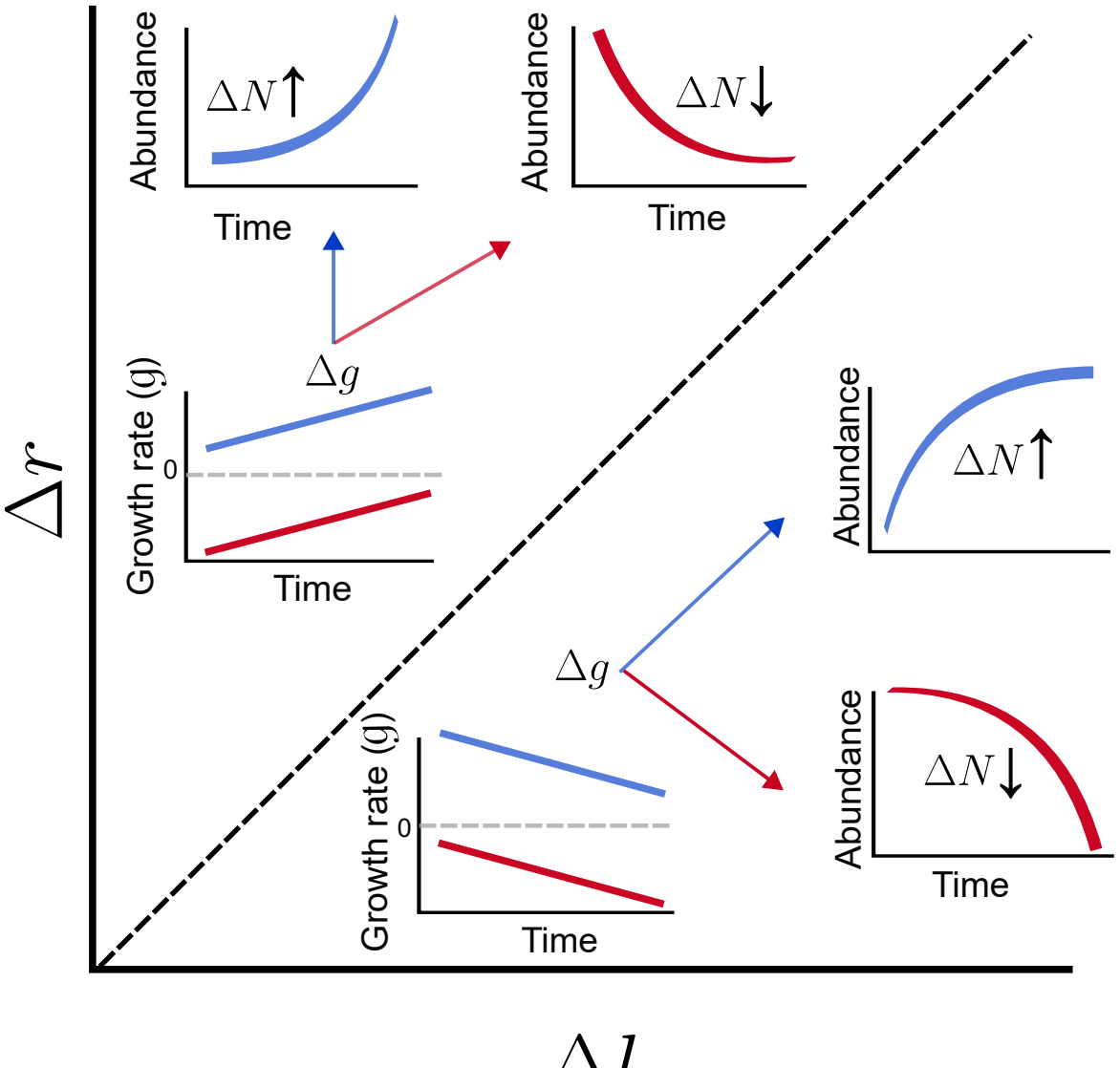

C

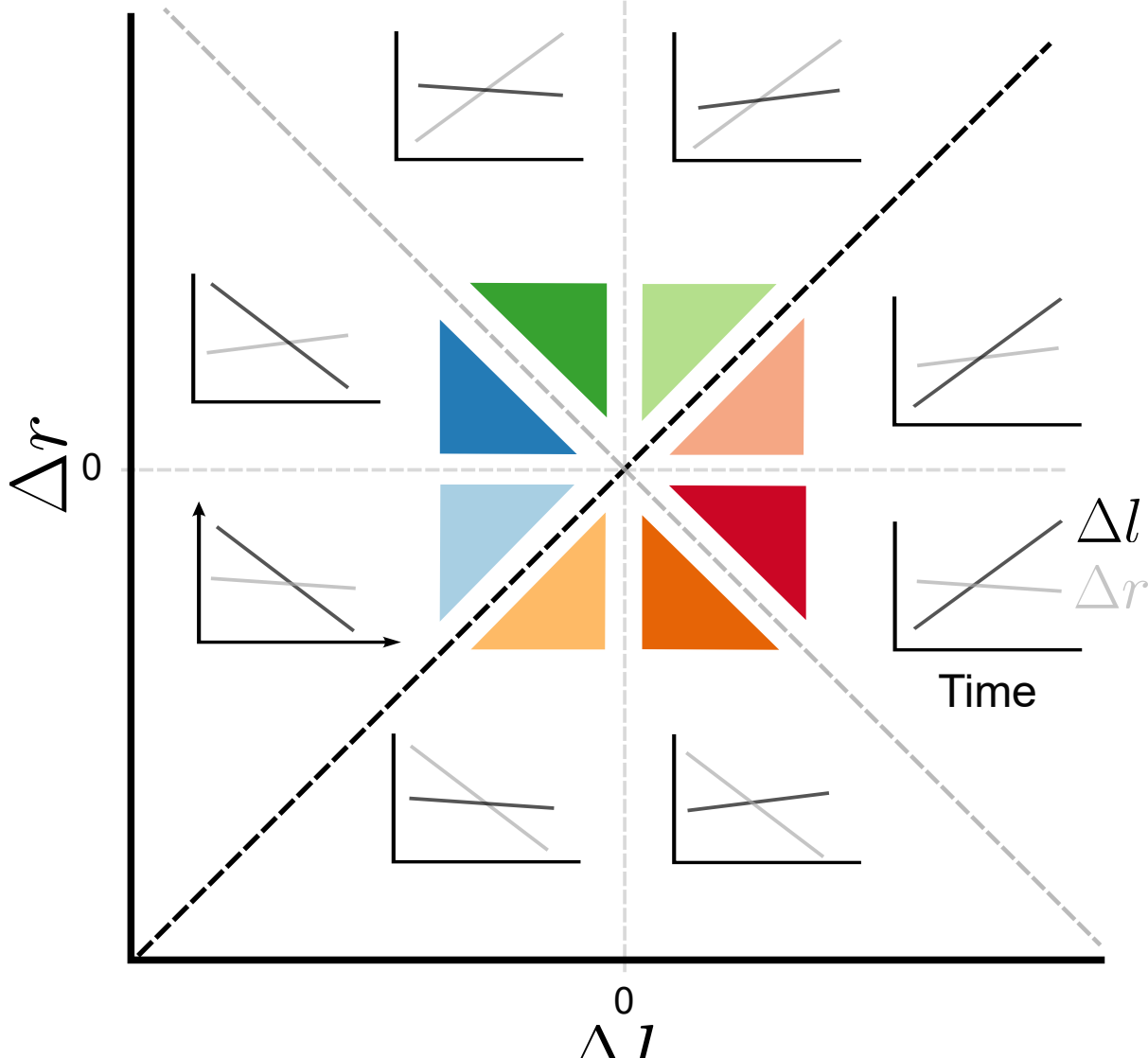

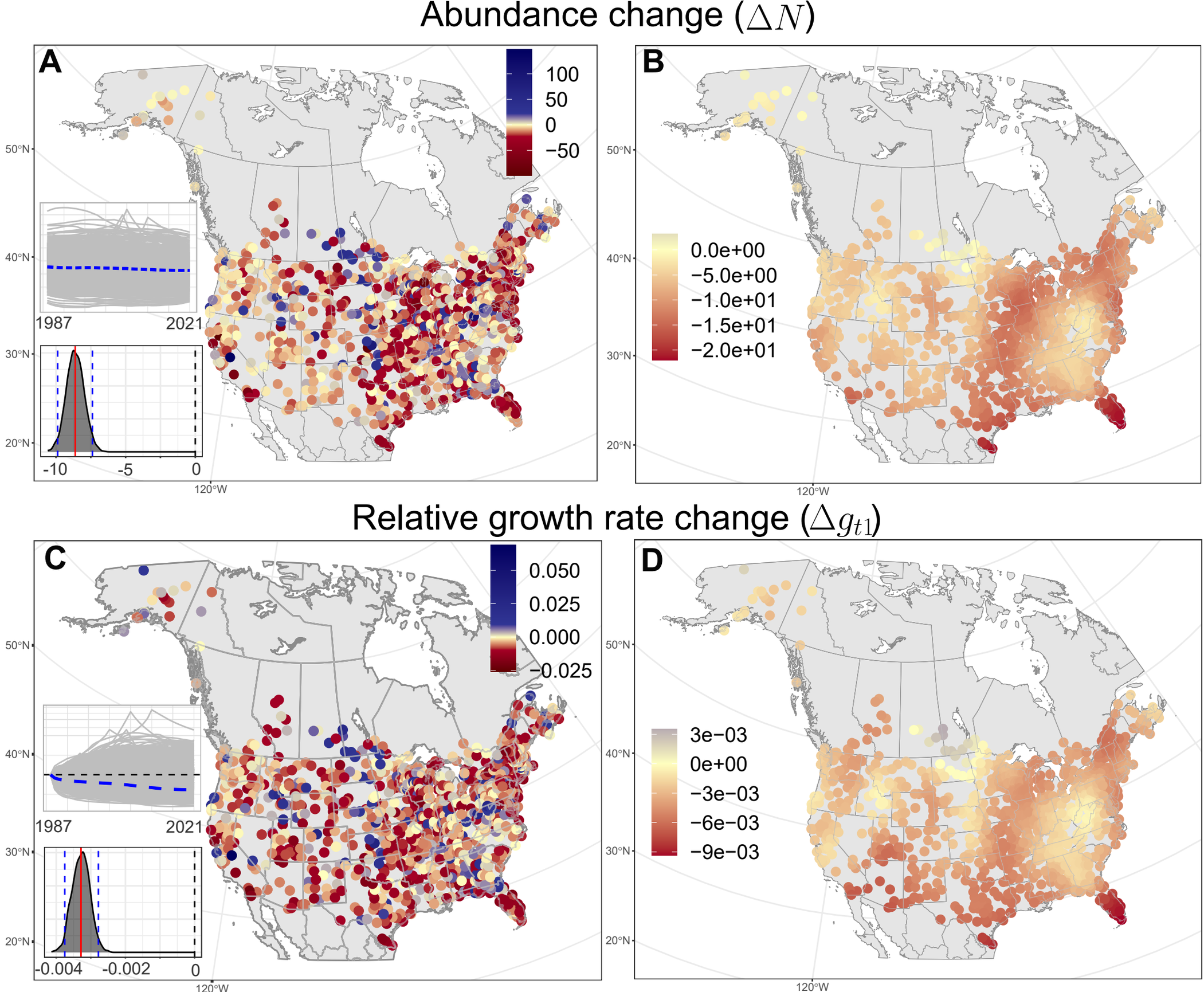
Abundance change (ΔN)
A
100
50
0
−50
1987
2021
-10
-5
0
50°N
40°N
30°N
20°N
120°W
B
0.0e+00
−5.0e+00
−1.0e+01
−1.5e+01
−2.0e+01
Relative growth rate change (Δg_{t1})
C
0.050
0.025
0.000
−0.025
-0.004
-0.002
0
D
3e−03
0e+00
−3e−03
−6e−03
−9e−03

Growth rate change ($\triangle g$)

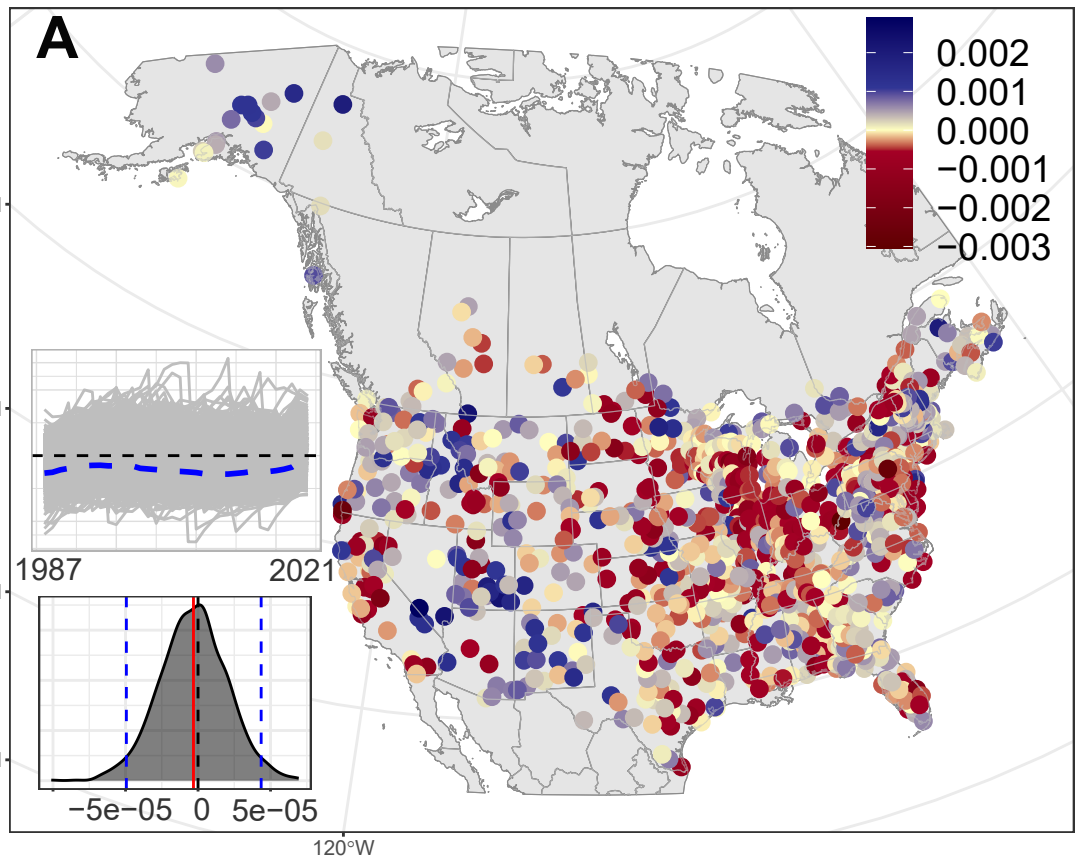

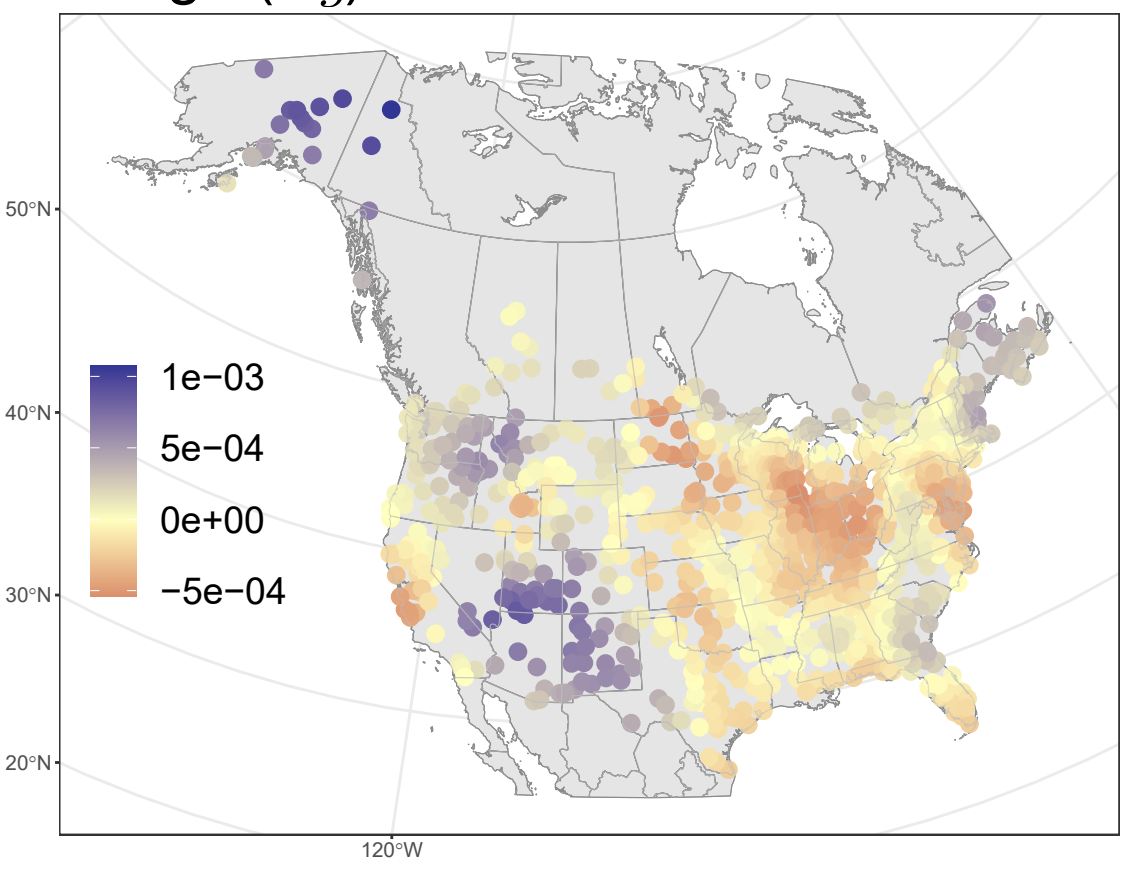

Recruitment rate change ($\triangle r$)

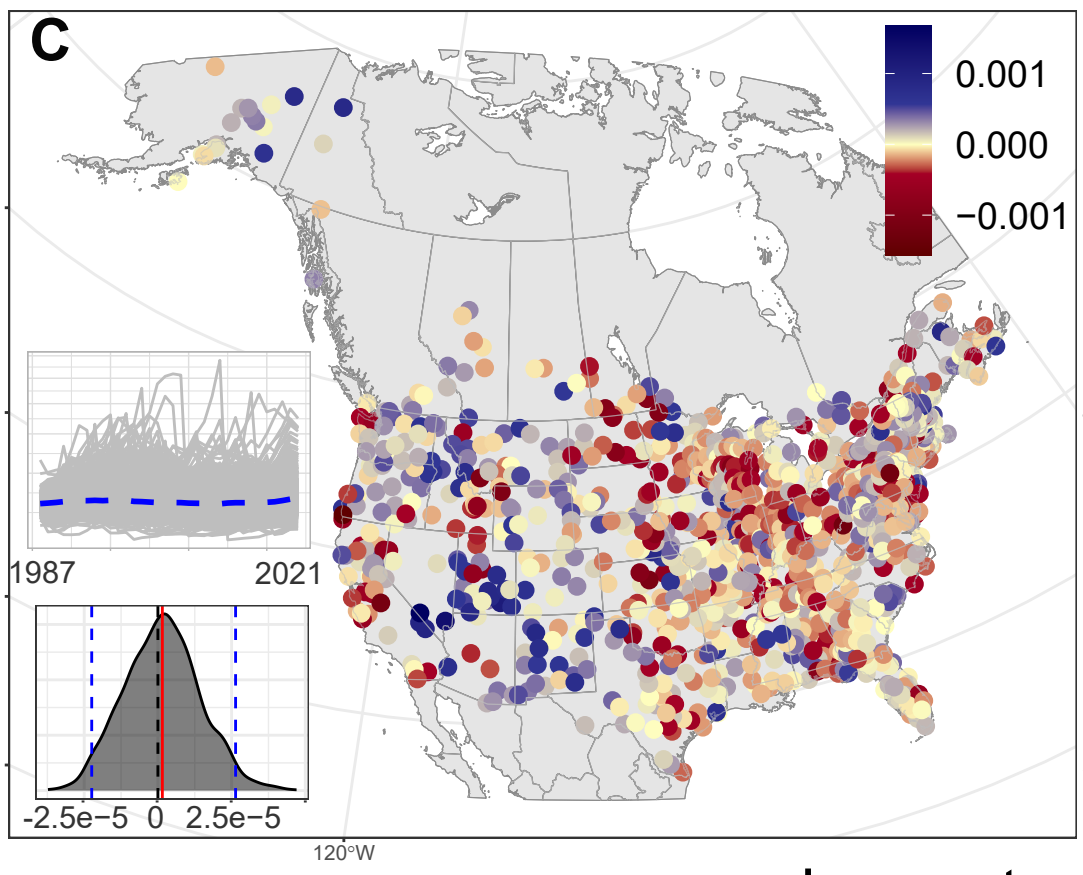

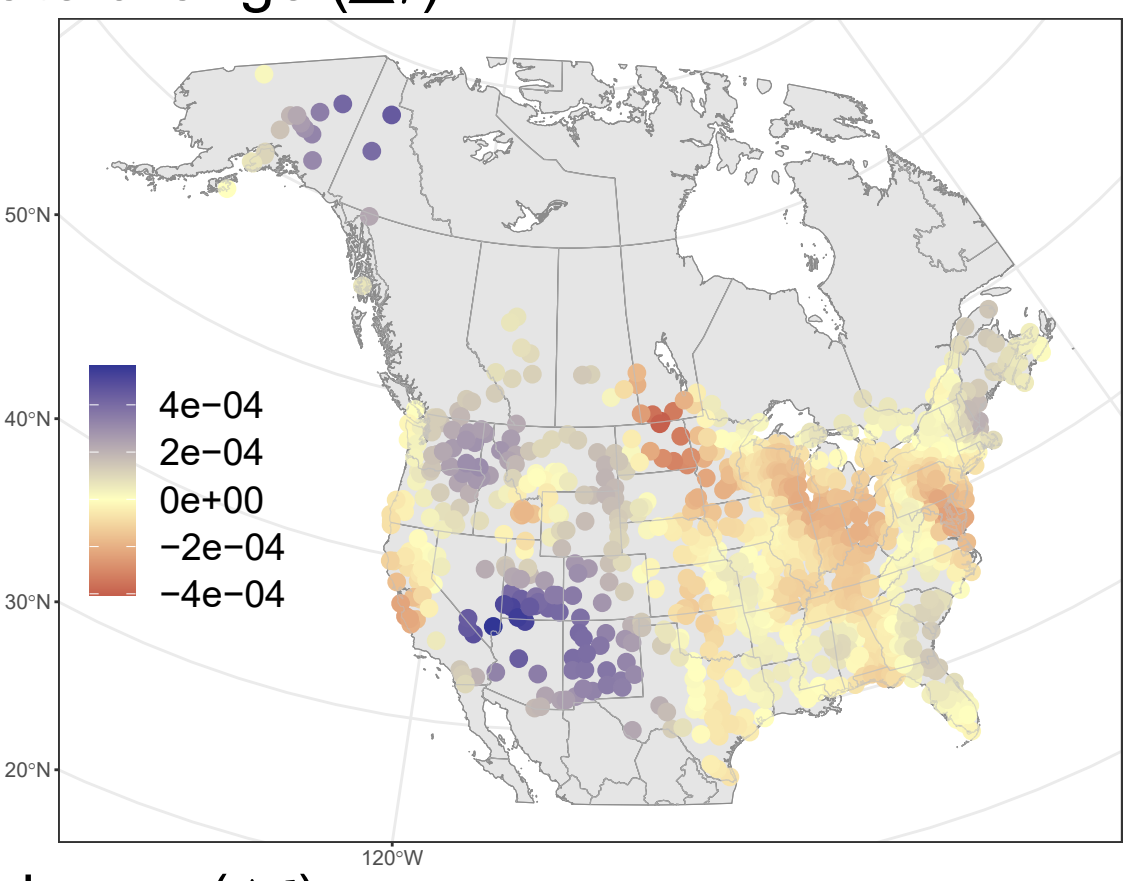

Loss rate change ($\triangle l$)

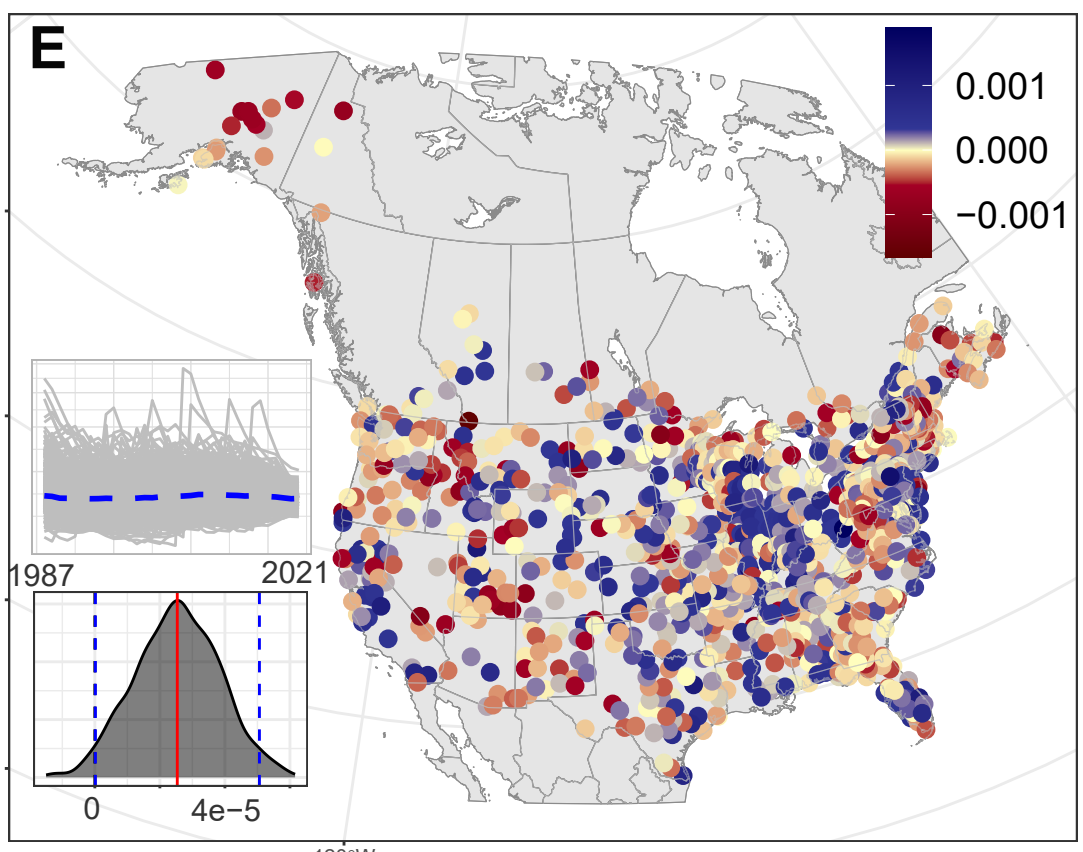

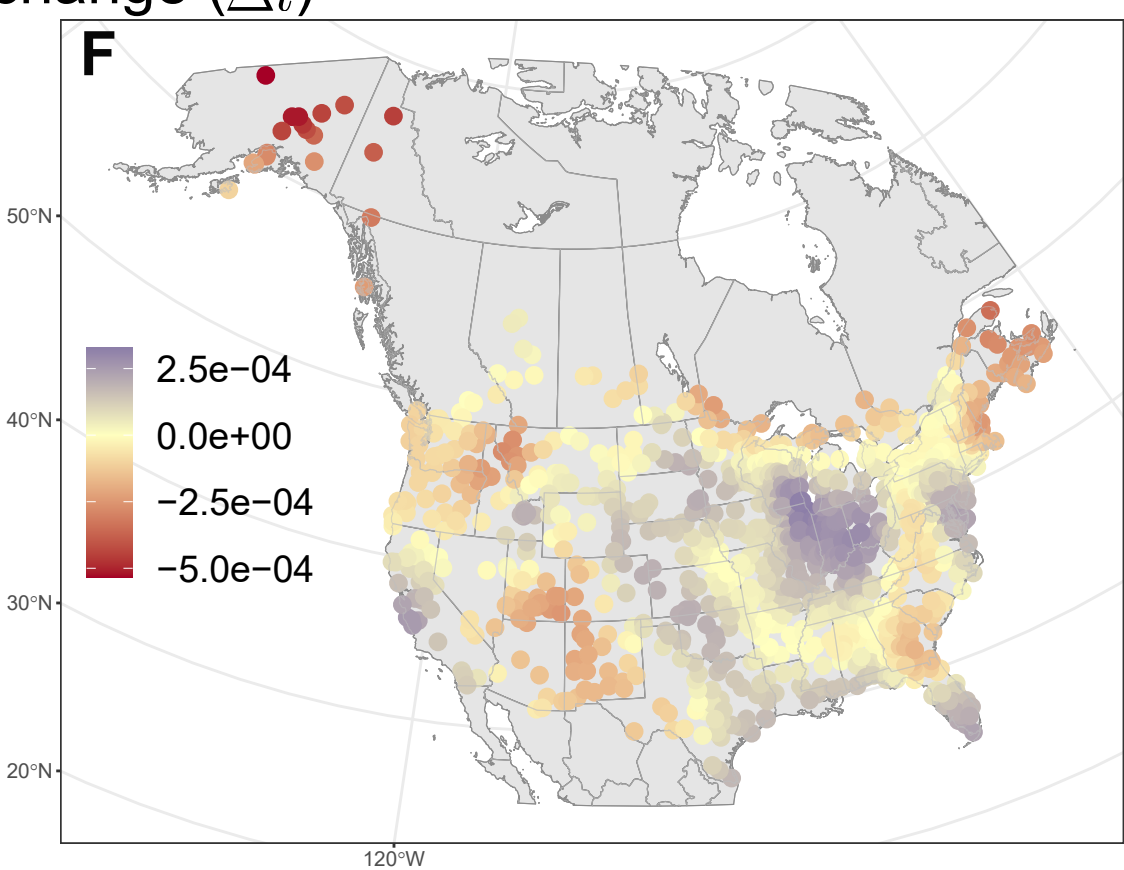

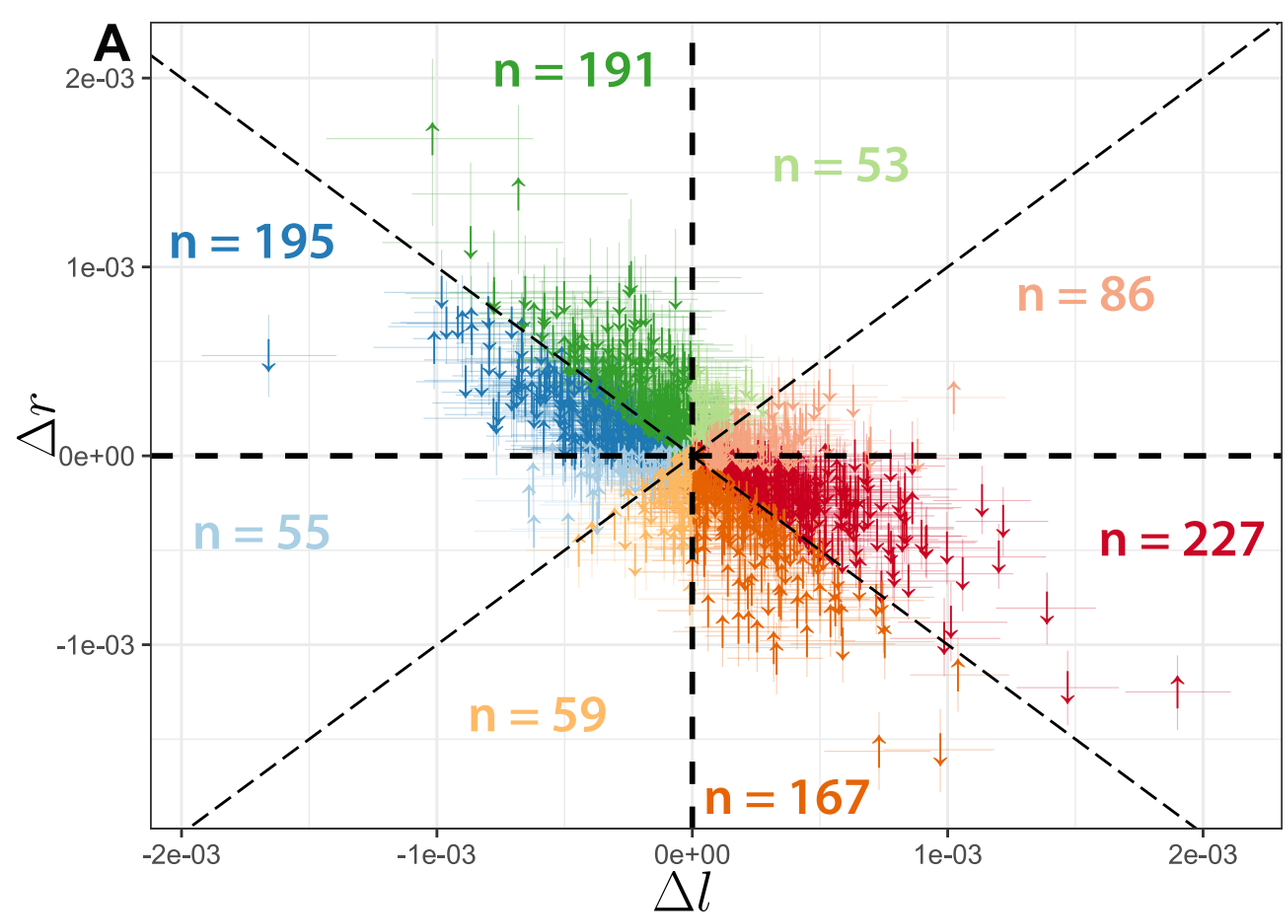
A
n = 191
n = 53
n = 195
n = 86
n = 55
n = 227
n = 59
n = 167
2e-03
1e-03
0e+00
-1e-03
-2e-03
-1e-03
0e+00
1e-03
2e-03
Δr
Δl

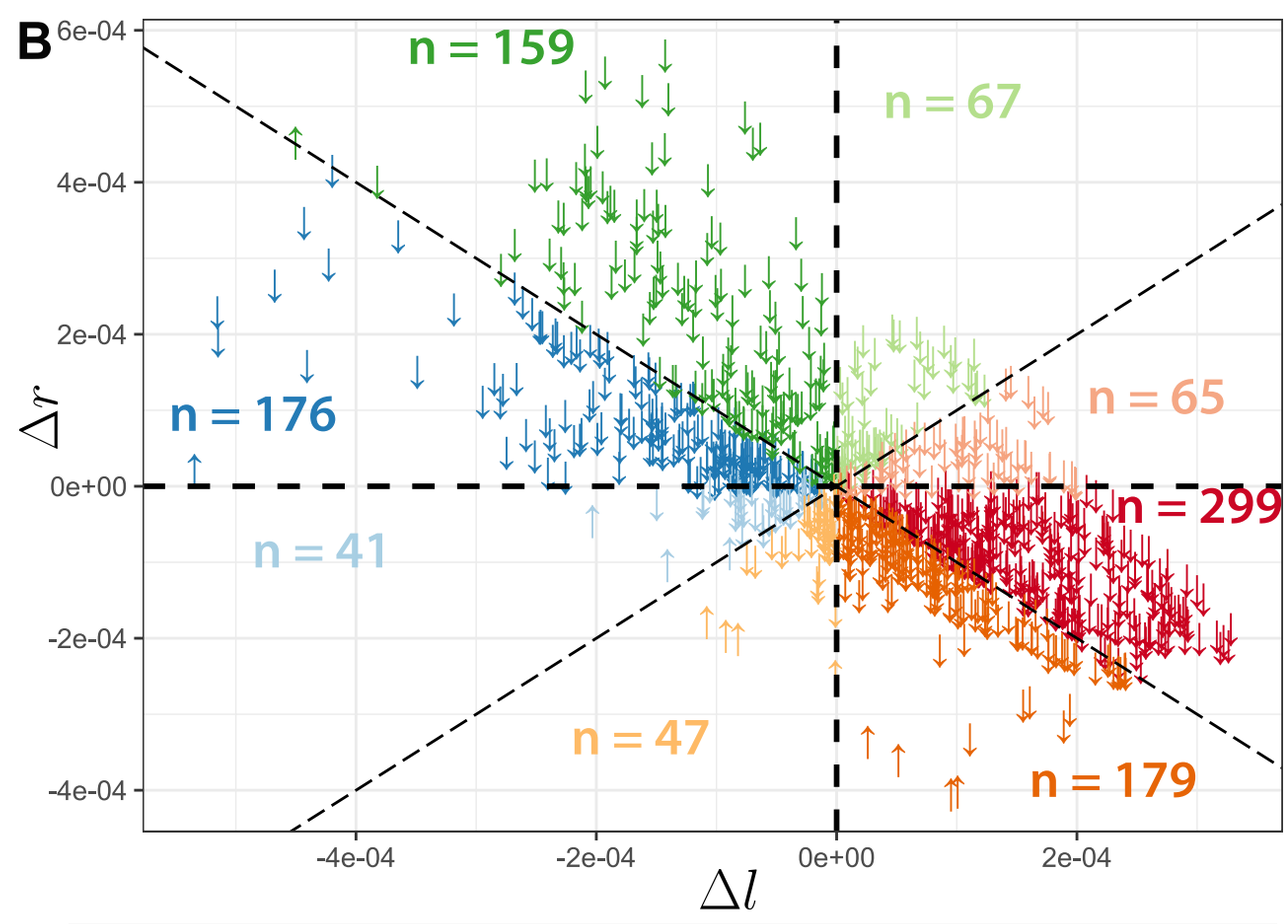
B
n = 159
n = 67
n = 176
n = 65
n = 41
n = 299
n = 47
n = 179
6e-04
4e-04
2e-04
0e+00
-2e-04
-4e-04
-4e-04
-2e-04
0e+00
2e-04
Δr
Δl

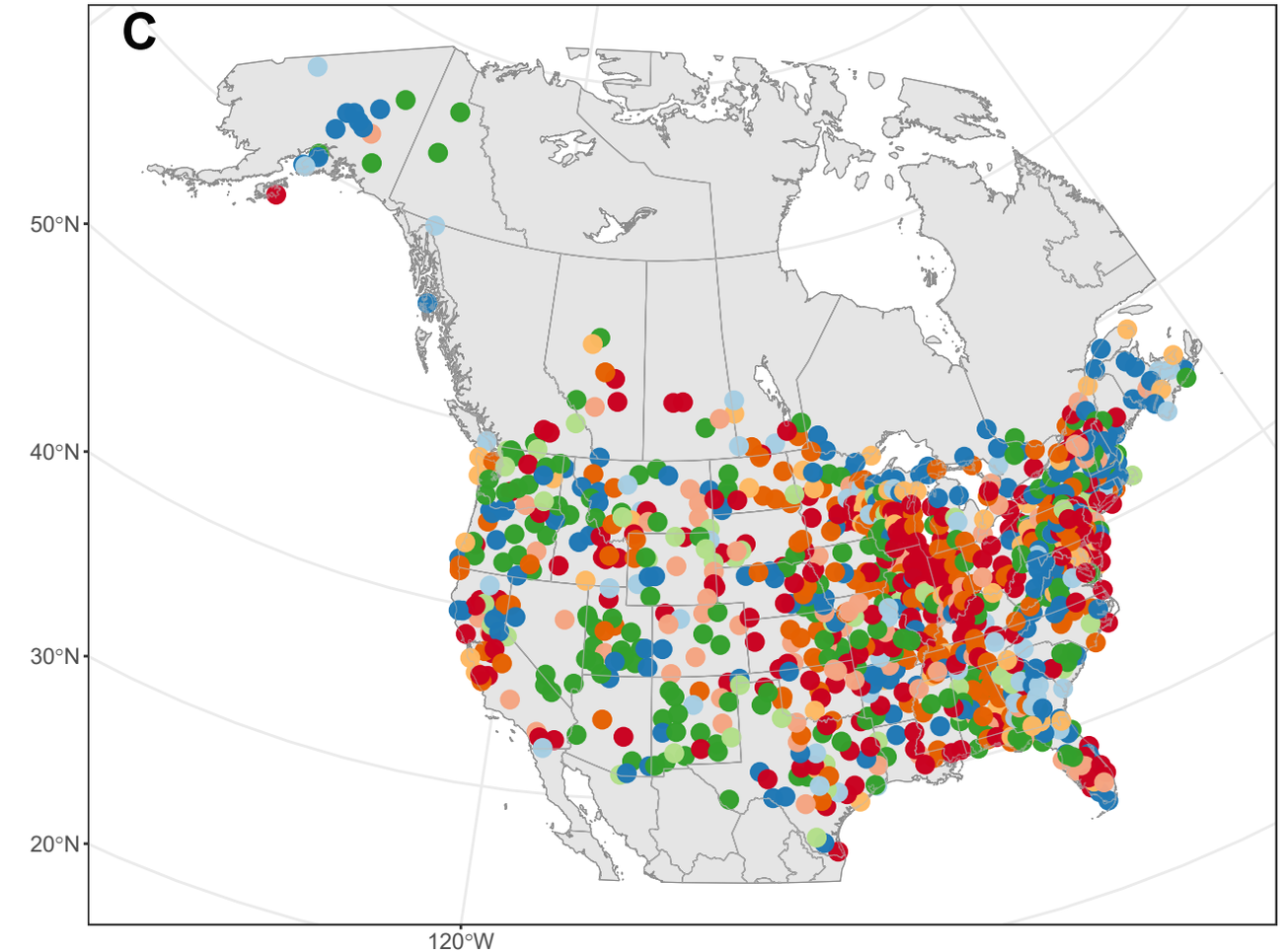
C
50°N
40°N
30°N
20°N
120°W

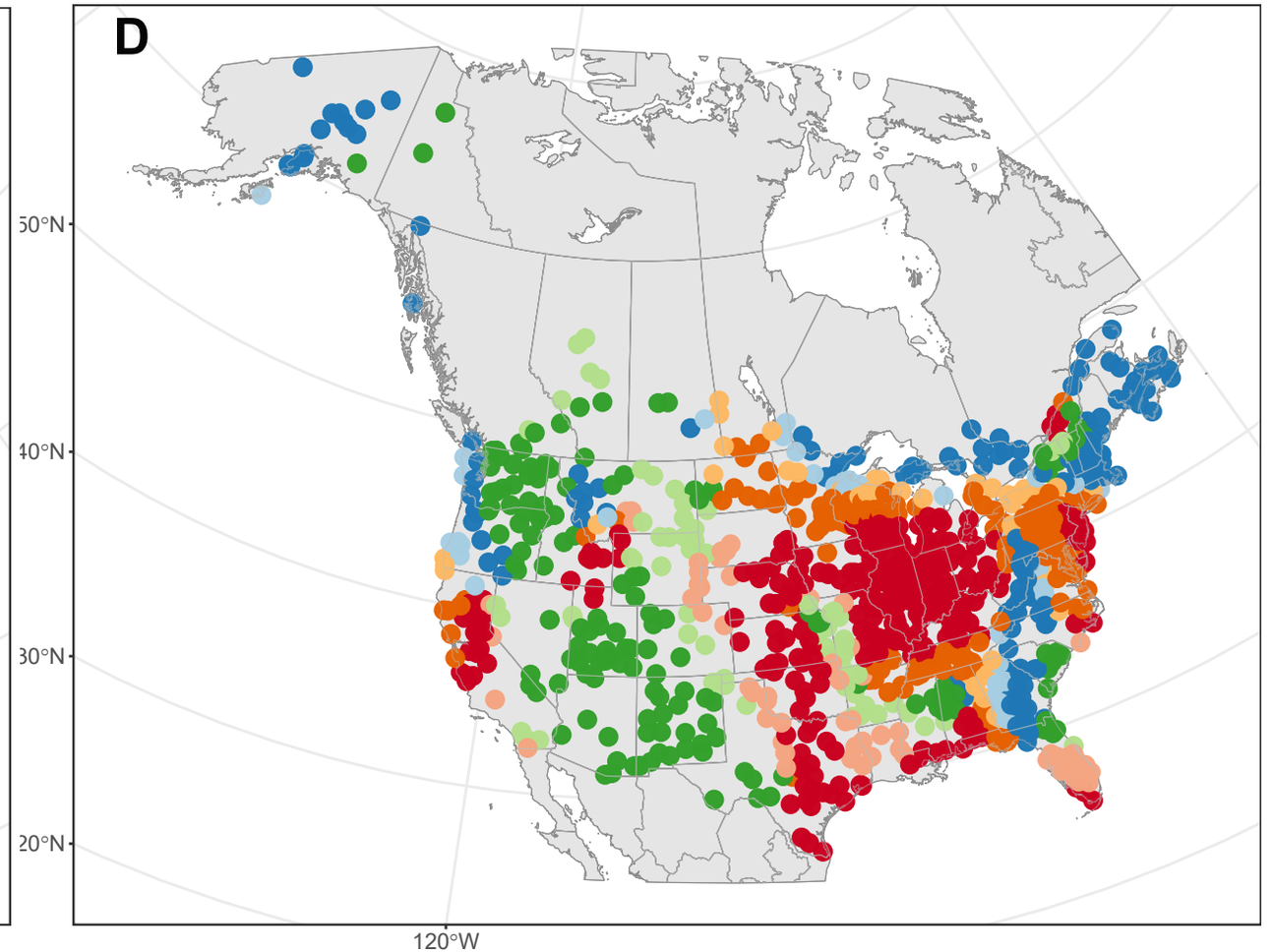
D
50°N
40°N
30°N
20°N
120°W

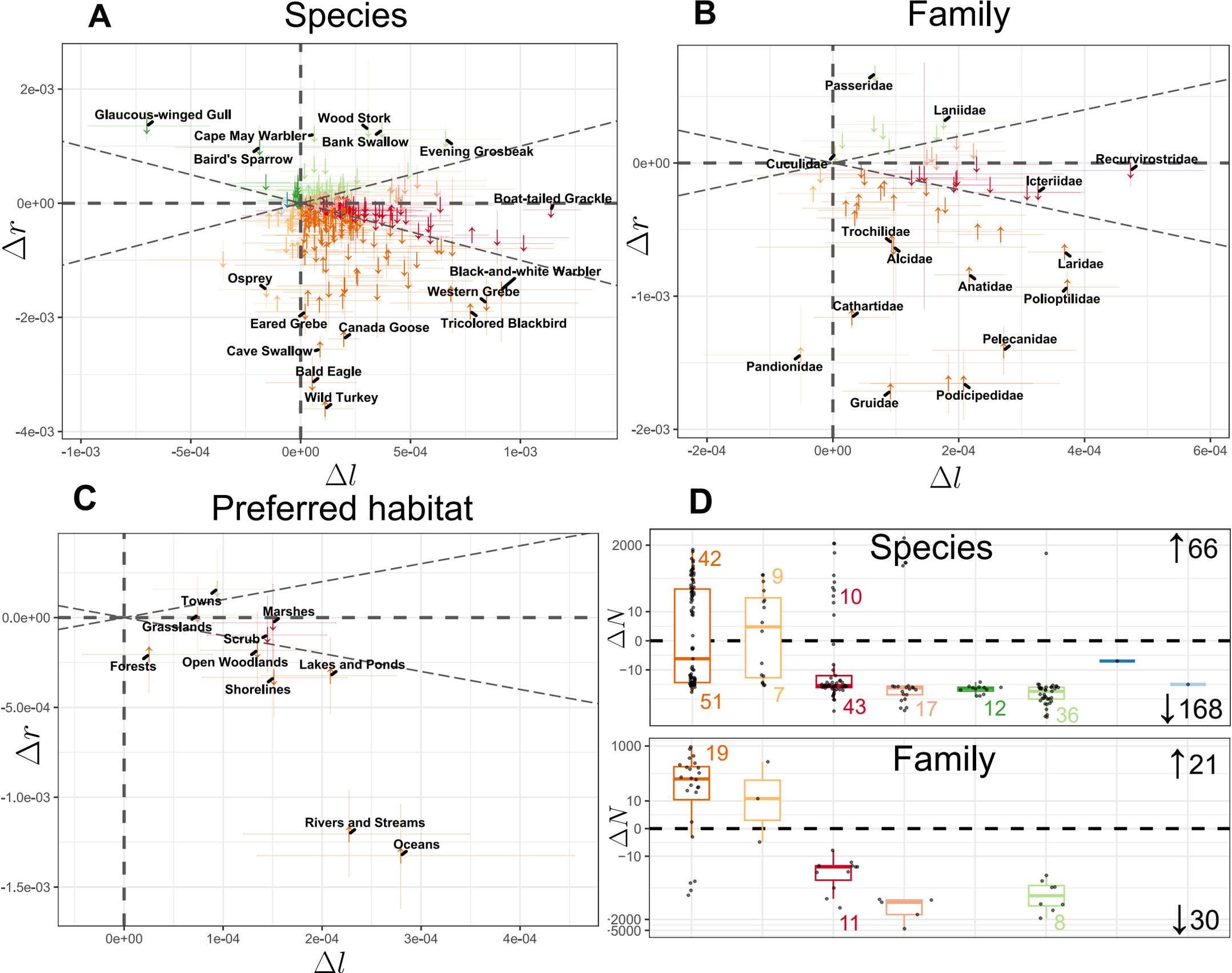
A
Species
Glaucous-winged Gull
Wood Stork
Cape May Warbler
Bank Swallow
Baird's Sparrow
Evening Grosbeak
Boat-tailed Grackle
Black-and-white Warbler
Osprey
Western Grebe
Eared Grebe
Canada Goose
Tricolored Blackbird
Cave Swallow
Bald Eagle
Wild Turkey
2e-03
0e+00
-2e-03
-4e-03
-1e-03
-5e-04
0e+00
5e-04
1e-03
Δr
Δl
B
Family
Passeridae
Laniidae
Cuculidae
Recurvirostridae
Icteriidae
Trochilidae
Alcidae
Laridae
Anatidae
Polioptilidae
Cathartidae
Pelecanidae
Pandionidae
Podicipedidae
Gruidae
0e+00
-1e-03
-2e-03
-2e-04
0e+00
2e-04
4e-04
6e-04
Δr
Δl
C
Preferred habitat
Towns
Marshes
Grasslands
Scrub
Forests
Open Woodlands
Lakes and Ponds
Shorelines
Rivers and Streams
Oceans
0.0e+00
-5.0e-04
-1.0e-03
-1.5e-03
0e+00
1e-04
2e-04
3e-04
4e-04
Δr
Δl
D
Species
↑66
↓168
42
9
10
51
7
43
17
12
36
2000
10
0
−10
ΔN
Family
↑21
↓30
19
11
8
1000
10
0
−10
−2000
−5000
ΔN